



**Quantifying water saturation in  
steel pipes using X-rays**

by

Haraldur Sigurðsson

Thesis

**Master of Science in Sustainable Energy**

January 2012



# **Quantifying water saturation in steel pipes using X-rays**

Haraldur Sigurðsson

Thesis submitted to the School of Science and Engineering  
at Reykjavík University in partial fulfillment  
of the requirements for the degree of  
**Master of Science in Sustainable Energy**

January 2012

## Supervisor(s):

Haraldur Auðunsson, Supervisor  
Associate Professor, Reykjavík University, Iceland

Guðrún Arnbjörg Sævarsdóttir, Supervisor  
Associate Professor, Reykjavík University, Iceland

## Examiner(s):

Gissur Örlygsson, Examiner  
Project Manager, Innovation Center Iceland

## **Abstract**

X-ray imaging equipment, moveable C-beam available at Biomedical engineering lab at Reykjavík University, was used to quantify the liquid fraction in steel pipes filled with different materials. The experiments were done using steel pipes of different diameter and wall thickness and preliminary results showed that useful X-ray images could not be obtained with wall thickness greater than 8 mm, most likely because of limited energy of the beam (max 106 keV). X-ray penetration was sufficient when pipe diameter was limited to 100 mm, while there was rock material inside the pipe, and thickness less than 8 mm. Using image software to evaluate the images from the experiments, it was observed that as water was added into the pipe the greyscale of the image changed gradually. To obtain an absolute scale for the greyscale of the images, a step wedge made of steel was used. This method was used on several pipes but the one that fitted the X-ray equipment best was a pipe with diameter 76 mm and wall thickness 4,5 mm. The pipe was subsequently filled gradually with water while taking X-ray images every step of the way and also filled with angular quartz fragments and basalt material in an effort to simulate a geothermal reservoir. This experiment shows that X-ray imaging can be used, along with absorption reference for comparison (step wedge), to quantify water saturation in steel pipes. It can therefore be concluded that experiments done to measure for example steam-water relative permeability can be performed at higher pressure than before, which is desirable when mimicking conditions in geothermal reservoirs.

## Útdráttur

Röntgen búnaður, færanlegt C-bómu röntgentæki sem er tiltækt á rannsóknarstofu heilbrigðisverkfræði Háskólans í Reykjavík, var notaður til að magntaka vökva hluta í stálrörum sem fyllt voru mismunandi efnum. Tilraunirnar voru gerðar með nokkrum stálrörum af mismunandi sverleika með mismunandi veggþykkt og við forrannsókn kom í ljós að nothæfar myndir náðust ekki af röri með veggþykkt yfir 8 mm, sem takmarkast líklega af orku röntgengeislans (max 106 keV). Smýgni röntgengeislans var ágæt þegar þvermál röranna var takmörkuð við 100 mm, þegar það innihélt steinefni, og veggþykkt minni en 8 mm. Myndvinnsluforrit var notað til að meta myndirnar frá tilraununum, þar sem sást að eftir því sem vatnsmagn var aukið í rörinu þá dökknaði myndin (gráskalinn breyttist). Til að hafa fasta viðmiðun fyrir gráskala á myndunum þá var búin til trappa úr stáli sem höfð var með á myndunum. Þessi aðferð var notuð við öll rörin í tilrauninni en það rör sem passaði best við röntgenbúnaðinn var með 76 mm þvermál og veggþykkt 4,5 mm. Vatni var hellt smátt og smátt inn í rörið og röntgenmyndir teknar reglulega þar til rörið var fullt en einnig var annars vegar kvarts og hinsvegar basalt sett í rörið til að líkja eftir jarðhita forðageymi. Þessar tvær begtegundir voru notaðar til að kanna hvaða áhrif efnasamsetning jarðefnisins hefði á gleypni þess fyrir röntgen geislann, en efnasamsetning kvartsins er aðallega  $\text{SiO}_2$  og því úr léttari frumefnum en basaltið sem inniheldur meira af þyngri efnum, meðal annars málum. Þessi tilraun sýnir að hægt er að nota röntgentæki, með því að hafa viðmiðunar tröppu, til að finna vatnsmagn í röri. Það þýðir að tilraunir sem til dæmis er ætlað að mæla hlutlekt vatns og gufu, er hægt að gera við hærri þrýsting en hingað til. Það hefur gildi þegar verið er að reyna að líkja eftir ástandi í jarðhita forðageymi, þar sem tvífasa jarðhitavökvi streymir við háan þrýsting.

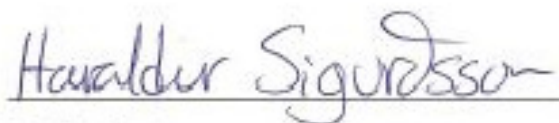
# Quantifying water saturation in steel pipes using X-rays

Haraldur Sigurðsson

Thesis submitted to the School of Science and Engineering  
at Reykjavík University in partial fulfillment  
of the requirements for the degree of  
**Master of Science in Sustainable Energy**

January 2012

Student:

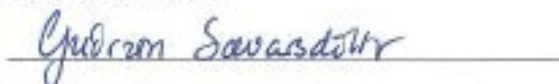


Haraldur Sigurðsson

Supervisor(s):



Haraldur Auðunsson



Guðrún Arnbjörg Sævarsdóttir

Advisor:



María Sigríður Guðjónsdóttir

Examiner:



Gissur Örlygsson

## **Acknowledgements**

I want to express my sincere gratitude to my supervisors, Haraldur Auðunsson and Guðrún Arnbjörg Sævarsdóttir for their support and guidance throughout this thesis work and of course also María Sigríður Guðjónsdóttir for reading through the work, commenting and helping on this thesis. The teachers at both Reykjavík University and University of Iceland also deserve thanks for their part in teaching and inspiring me in class. I would also like to thank my fellow master student and friend Jón Rafn Valdimarsson for his help throughout this master studies period. I dedicate this work to my family who has always supported me and encouraged in everything I have done.

## Table of Contents

1	Introduction .....	1
1.1	Experiments using X-rays .....	2
1.2	Project goals and objectives .....	5
2	Theoretical background.....	6
2.1	X-rays .....	6
2.2	Interaction with matter.....	9
2.2.1	Interaction mechanism .....	9
2.2.2	Interaction of X-ray with matter and rate of attenuation.....	11
2.3	Neutron logs .....	13
3	Experiment setup.....	15
3.1	Steel pipes.....	15
3.2	Imaging equipment .....	16
3.3	Step wedge.....	18
3.4	Image processing .....	19
3.5	Rack for the pipes and rock material .....	20
4	Measurements.....	21
4.1	Pipe nr. 1 .....	22
4.2	Pipe nr. 2.....	23
4.3	Pipe nr. 3.....	24
4.3.1	Neutron logging with pipe nr. 3 .....	24
4.4	Pipe nr. 4.....	25
4.5	Pipe nr. 5.....	30
4.6	Pipe nr. 6.....	32
4.6.1	Neutron logging with pipe nr. 6 .....	33
5	Discussions.....	35
6	References .....	38

## Table of Figures

Figure 1: 1904, Prince Ginori Conti and the 10 kW experimental power plant in Larderello, Italy (J. W. Lund, 2004). .....	1
Figure 2: a) (Corey, 1954) (solid line) and linear (dashed line) relative permeability curves, b) Results from Ambusso's experiments. $K_r$ is relative permeability and $S_w$ is saturation of water (Horne et al., 2000). .....	4
Figure 3: a) Results from Satik (1998) and b) Results from Mahiya (1999), which both look like fitting the Corey curve $K_r$ is relative permeability and $S_w$ is water saturation (G. F. Mahiya, 1999; Satik, 1998). .....	5
Figure 4: Spectrum of electromagnetic radiation ( <i>Berkeley lab</i> , n.d.). .....	7
Figure 5: Schematic of an X-ray tube (Simmons, n.d.). .....	7
Figure 6: Bremsstrahlung and Characteristic radiation ( <i>CT physics</i> , 2006). .....	8
Figure 7: Energy spectrum of an x-ray beam generated in an X-ray tube, $K_\alpha$ and $K_\beta$ are due to L-shell and M-shell drops respectively (Wolbarst, 2005, p. 301). .....	9
Figure 8: Interactions of x-ray with matter (Wolbarst, 2005, p. 91). .....	10
Figure 9: Absorption probability of photons while travelling through water for different photon energies (Sternheim & Kane, 1991, p. 829). .....	11
Figure 10: Travelling of an x-ray beam through a slab (Wolbarst, 2005, p. 153). .....	12
Figure 11: Cross section of pipe nr. 4 (see chapter 9.4) and the results of calculations of the beam intensity through the pipe for at the effective energy calculated at page 35. ....	13
Figure 12: Neutron well logging device in a borehole, there is usually a bracket that presses the device up against the wall of the borehole so that it can obtain data from the strata the borehole goes through (Ellis, 1990). .....	14
Figure 13: Pipe with welded ends. ....	15
Figure 14: Pipe fitted with Plexiglas end with ruler attached. ....	16
Figure 15: Photos of the X-ray machine and the experiment setup in the Biomedical engineering lab at Reykjavík University. ....	16
Figure 17: a) Image taken with no screening, b) Image taken with screening and a step wedge .....	17
Figure 16: TV-screens that display the images from the X-ray machine. ....	17
Figure 18: Photo of step wedges, a) First version b) Second version. ....	19
Figure 19: Step wedge, final version made with sheet metal, 9 steps 0.8mm each. ....	19
Figure 20: Demonstration of how the greyscale values are obtained for different regions in ImageJ. ....	20



Figure 21: Photos of the material used in the experiments, a) Quartz ca. 5 – 30 mm and b) Basalt gravel 3 – 5 mm (memory stick for size comparison).....	21
Figure 22: Photos from the pilot study with pipe nr. 1, a) Pipe nr. 1 near the image intensifier tube, b) Image from the X-ray machine. ....	22
Figure 23: Series of images from experimenting with pipe nr. 1 OD 89,1 a) No water, b) Water height in pipe 18 mm, c) Water height 43 mm, d) Water height 66 mm. ....	22
Figure 24: Images from the pilot study using pipe nr. 2, a) The setup, b) Image from the X-ray machine and the water level is barely visible.....	23
Figure 25: Photos from the pilot study with pipe nr. 3, a) The setup, b) Image from the X-ray machine showing that the water level is visible. ....	24
Figure 26: Pipe nr. 3 in a neutron logger experiment.....	25
Figure 27: a) Image from the pilot study showing the setup, b) Image from preliminary experiment with few pieces of Quartz in the pipe.....	25
Figure 28: Results from experimenting with pipe nr. 4 filling it gradually with water and making X-ray images at every step at 106 keV and 6,4 mA.....	26
Figure 29: Results from experimenting with pipe nr. 4 full of Quartz material and then filling it gradually with water and making X-ray images at every step at 106 keV and 6,4 mA.....	28
Figure 30: Results from experimenting with pipe nr. 4 full of Basalt material and then filling it gradually with water and making X-ray images at every step at 106 keV and 6,4 mA.....	29
Figure 31: a) Pipe nr. 5, b) Image from the X-ray machine and the Quartz level is visible and but the X-rays did not penetrate the Quartz as needed and the greyscale value for the region of interest was only 14,5.....	30
Figure 32: Results from the first experiment with pipe nr. 5 filling it gradually with water and making X-ray images at every step at 106 keV and 6,4 mA, no rock material.....	31
Figure 33: a) photo of pipe nr. 6 b) Image from the X-ray machine where the Quartz level is visible but the X-rays did not penetrate the cross section of the pipe filled with Quartz. ....	32
Figure 34: Schematic of how the diameter of pipe nr. 6 would have been changed to get image of the middle of the pipe. ....	32
Figure 35: Results from a neutron logger at a well with casing to approximately 35 m depth. ....	33
Figure 36: Results from experimenting with neutron logger and pipe nr 6 filling it gradually with water.....	34
Figure 37: Neutron experiment setup giving the results in Figure 36.....	34
Figure 38: Sketch of proposed neutron logger experiment. ....	35

## List of Tables

Table 1: Mass attenuation coefficients and Linear attenuation coefficients for a few materials at four different energies (Siegbahn, 1955).....	13
Table 2: Pipes used in the experiments .....	15
Table 3: Attenuation for Iron and Water at different energies. ....	28

## List of constants and variables

$\lambda$	Wavelength [m]
$f$	Frequency [Hz]
$E$	Energy [J]
$h$	Planck's constant $\approx 6,626 \cdot 10^{-34} [J \cdot s]$
$c$	Speed of light in vacuum $\approx 2,99 \cdot 10^8 [\frac{m}{s}]$
$eV$	electron volt $1eV = 1.602 \cdot 10^{-19} [J]$
$\text{\AA}$	Ångström ( $10^{-10}$ m) Wavelength measurement
$E_L$	Energy of electron on L-shell [eV]
$E_K$	Energy of electron on K-shell [eV]
$d$	Length of cross section [m]
$I_{in}$	Intensity of incoming X-ray beam [ $W/m^2$ ]
$I_{out}$	Intensity of outgoing X-ray beam [ $W/m^2$ ]
$\mu$	Linear attenuation coefficient [ $cm^{-1}$ ]
$\mu_m$	Mass attenuation coefficient [ $cm^2/g$ ]
$\sigma$	Energy density spectrum [J]
$\Sigma$	Macroscopic cross section of material [ $m^2$ ]
$L_s$	Slowing-down length [m]
$k_r$	Relative permeability [ $m^2$ ]
$S_w$	Saturation of Water
$v_w$	Velocity of water [m/s]
$v_s$	Velocity of steam [m/s]

$k_{rs}$	Relative permeability of steam [ $m^2$ ]
$k_{rw}$	Relative permeability of water [ $m^2$ ]
$\dot{m}$	Mass flow of fluid [kg/s]
$\nu$	Fluids kinematic viscosity [ $m^2/s$ ]
$\rho_w$	Density of water [kg/ $m^3$ ]
$\rho_s$	Density of steam [kg/ $m^3$ ]
$g$	Earth's gravitational acceleration [ $m/s^2$ ]
$\mu$	Dynamic viscosity [ $kg / m \cdot s$ ]
$S_v$	Equivalent dose (of ionizing radiation) [Sievert]
$p_c$	Pressure [Pa]
$e$	Wall thickness [m]
$f_c$	Design stress [Pa]
$D_o$	Outer diameter of pipe [m]
API	American Petroleum institute

# 1 Introduction

There is no way of directly measuring the temperature of the Earth's core but the temperature at the centre of the inner core of the earth has been estimated to be around 6600°C and the molten rock in the mantle that is under the relatively thin crust around 2200°C (DiPippo, 2008, p. xix). The most significant source of heat in the Earth's interior are radioactive elements, in particular potassium, uranium and thorium (Sanders, 2003). Normal temperature gradient from the surface of the Earth into the crust is around 3°C per 100 m but there are areas where this does not apply. At some locations of the Earth there is volcanic or tectonic activity where the molten rock from the mantle gets close to the surface and heats it up. In such areas the thermal gradient can be 10-30 times higher than the normal temperature gradient mentioned (DiPippo, 2008, p. xix).

From the beginning of civilization hot springs in geothermal areas throughout the world have been utilized for bathing and washing clothes. Through the history, people in ancient civilization like the Greeks, Japanese, Maoris, Mexicans, Etruscans and Chinese were known to use hot springs, which were believed to have healing powers. Records show that people in China have been using geothermal water for over 2000 years and Roman baths were legendary throughout the empire at its peak. While hot water from geothermal areas has been utilized for bathing and washing for thousands of years it was not used to heat up buildings until the 14<sup>th</sup> century and the first district heating that utilized geothermal water was founded 1930 in Reykjavík, Iceland (Fridleifsson & Freeston, 1994).

First geothermal power plant that used geothermal power to produce electricity was built in Larderello region in Tuscany, Italy in 1904 and can be seen in Figure 1. In that plant an experimental 10 kW generator was used and by the end of 1943 the installed capacity was 132 MW but after heavy bombing in the Second World War the plant could only produce 23 kW (J. W. Lund, 2004).



Figure 1: 1904, Prince Ginori Conti and the 10 kW experimental power plant in Larderello, Italy (J. W. Lund, 2004).

In 2004 the capacity of electricity production by geothermal utilization had grown to about 9 GW in 25 countries, serving the equivalent of 60 million people (J. W. Lund, 2004).

To be able to use geothermal fluid for a sustainable power production in geothermal power plants, research is required on the geothermal reservoir that is going to be utilized. This research is done on the underlying strata by drilling a borehole (well), collecting bore drill chips from the well as well as using neutron loggers that measure porosity and resistivity loggers that show where fractures can be found in the strata. Combining the results from these logging equipments gives good information on the properties of the strata and the surroundings of the well. Quality of the reservoir is a determining factor: it should have a high temperature gradient or  $>200^{\circ}\text{C}/\text{km}$ , the size of it has to be sufficient for production for many years (decades) and the strata have to be porous and or they have to have good permeability and water has to be present (Fridleifsson & Freeston, 1994).

A Ph.D. project, by María S. Guðjónsdóttir, is now (January 2012) underway where conditions of a two phase flow of water and steam through a porous medium is measured. The goal of this Ph.D. project is to improve the relations that are currently used to describe two-phase flow through porous media. The traditional relations are the Darcy equations that assume the relative permeability to depend linearly on the water saturation (Horne et al., 2000).

An experimental apparatus has been built to measure the relative permeability of water and steam in a two phase flow through porous rock for a range of flow configurations and conditions. The main component of this experimental apparatus is a 4 m long steel pipe with 273 mm outer diameter and 5 mm wall thickness, which is filled up with rock material and steam and water is inserted at one end under pressure and flows out of other end at back pressure or atmospheric pressure. Due to resistance in the surrounding rock material, the fluid experiences pressure decline leading to increasing steam content since the flow is basically adiabatic. In the experiment, the pressure gradient will be measured and consequently the relative permeability is determined with respect to flow rates of the two phases (Guðjónsdóttir, Harvey, Pálsson, & Saevarsdóttir, 2010).

## **1.1 Experiments using X-rays**

X-rays have been used for medical purposes for over 100 years but they were discovered in 1895 by Dr. Röntgen who was a professor at the Wurzburg institute of physics in Germany. The X-rays and their ability to make an image of the bones within a living hand initially triggered a number of humorous plays in theaters and jokes in newspapers (Hessenbruch,

2002). During the initial X-ray craze the general public genuinely feared for losing their privacy and there were even advertisements that promised X-ray-proof underwear for sale. Some well known scientist even participated in séances measuring spiritualist mediums trying to see the unseen spirits they were connected to. Since the discovery of X-rays the development of the X-ray technology has been tremendous, many countries in Europe undertook mass screening of tuberculosis in 1930s and '40s. In 1960s new low dose examination was developed and mammography was expanded in an effort to detect breast cancer at early stages (Hessenbruch, 2002). In 1974 the CT (Computed Tomography) imaging systems were put on the market and since then there have been monumental changes in computer technology and what can be done today with CT imaging was unthinkable three decades ago (Hurlock, Higashino, & Mochizuki, 2009). X-rays have not only been used in medical application but they have also been used in a lot of experiments where scientists are discovering the structure of materials. Most common usage of X-rays outside medical applications is in non-destructive inspection of the internal soundness of welds. X-ray image of welding can show defects like bonding flaws, gas bubbles or cracks (Wang & Liao, 2002). At NASA, for example, CT was used for inspecting hydraulic accumulators that were suspected to have fatigue cracks that would lead to leakage of hydraulic fluids. Using CT for inspection made it possible to detect three levels of fatigue defects (Murray, 1990).

Geoscientists have also been using X-rays, mostly CT, to ascertain the internal structure of core samples, figure out flow in fractures, porosity of rocks and consequently their permeability. Numerous studies have been made in that field where these experiments were performed to realize the steam-water relative permeability as it says in the titles of most of the reports (W. J. Ambusso, 1996; Corey, 1954; Dastan, 2006; G. F. Mahiya, 1999; Satik, 1998). Repeated studies on this matter have had difficulty in producing consistent result because of the difficulty of determining the individual steam and water flow rates. The traditional Darcy equation, used to describe the mass flow for a horizontal one phase flow is shown in Eq. 1.

$$\dot{m} = -\frac{k}{\nu} A \frac{dp}{dx} \quad (1)$$

Where  $k$  is the intrinsic permeability of the surrounding porous media,  $\nu$  is the fluids kinematics viscosity and  $dp/dx$  is the pressure gradient of the flow. For a two phase flow the intrinsic permeability is not alone sufficient to account for the fluid permeability. A new factor is introduced, called the relative permeability,  $k_{rw}$  and  $k_{rs}$  for water and steam respectively. Equations (2) and (3) show the mass flow for the two phases in water and steam flow where the subscript w accounts for the water portion and s for the steam portion.

$$\dot{m}_w = -\frac{kk_{rw}}{v_w}A\frac{dp}{dx} \quad (2)$$

$$\dot{m}_s = -\frac{kk_{rs}}{v_s}A\frac{dp}{dx} \quad (3)$$

According to these Darcy equations it can be assumed that the relative permeabilities act as area reduction factors and can therefore be assessed as the phase saturation in the permeable matrix. That means that  $k_{rw}$  would be equal to the water saturation  $S_w$  and  $k_{rs}$  would be equal to  $1-S_w$ . Numerous studies have been conducted where the relative permeabilities have been calculated as a function of a measured water saturation, most of them contradict to the linear dependency suggested by the traditional Darcy equations.

In his report, Ambusso concluded that the steam-water relative permeabilities were best described with the (linear), X-curves see Figure 2 (Ambusso, 1996).

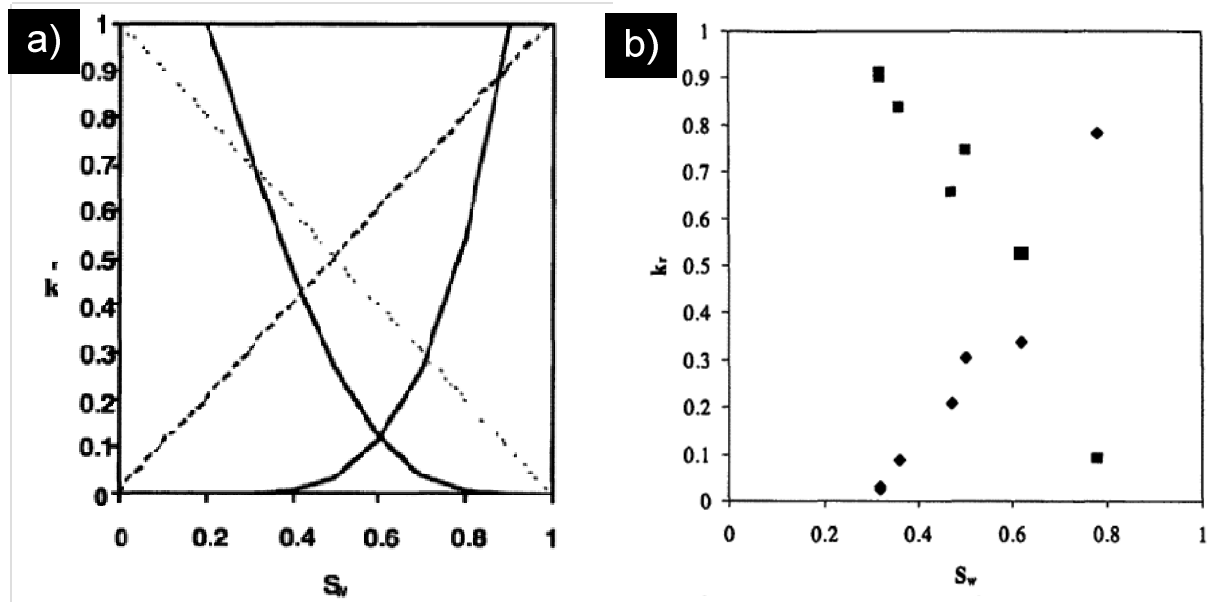


Figure 2: a) (Corey, 1954) (solid line) and linear (dashed line) relative permeability curves, b) Results from Ambusso's experiments.  $K_r$  is relative permeability and  $S_w$  is saturation of water (Horne et al., 2000).

Later studies (G. F. Mahiya, 1999; Satik, 1998), did not succeed in confirming these findings but instead indicated that Corey curve (as seen in Figure 2 a) was more likely fitting to the results as can be seen in Figure 3.

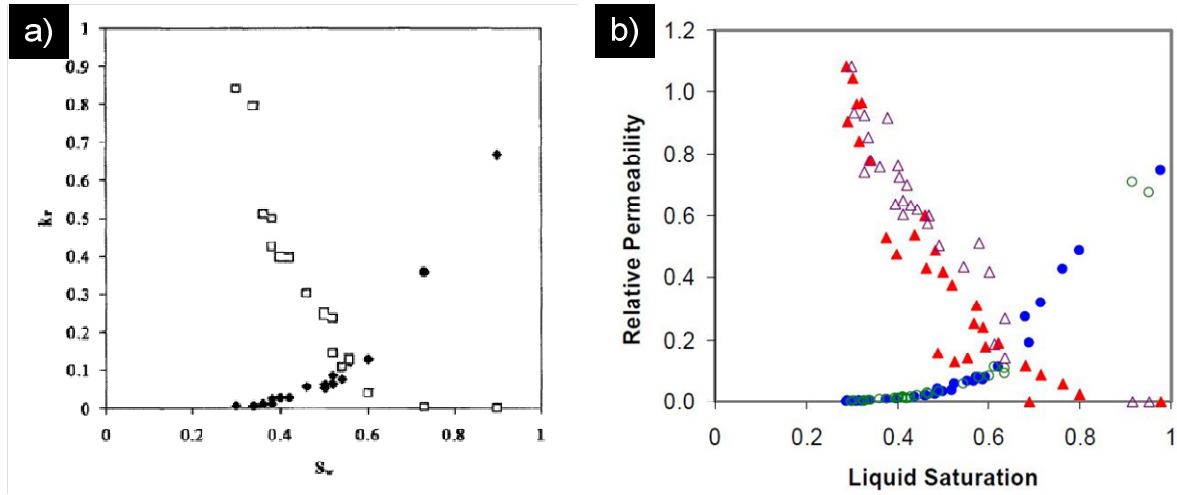


Figure 3: a) Results from Satik (1998) and b) Results from Mahiya (1999), which both look like fitting the Corey curve  $K_r$  is relative permeability and  $S_w$  is water saturation (G. F. Mahiya, 1999; Satik, 1998).

To be able to relate the relative permeability to water saturation, the water amount in the two phase flow has to be determined. Among other methods, X-ray has been used for saturation detection where flow of water and steam is inserted into a tube filled with rock material (Dastan, 2006; Horne et al., 2000; Schembre & Kavscek, 2003). Few experiments have been performed where the surrounding tube is made of metal material and the limitation of using of X-ray for detecting the water saturation in metal pipe filled with rock material is not fully known. Metal material is rather avoided in X-ray experiments because of its effects on the X-ray beam (severe attenuation and beam hardening) although thin Aluminium has been used (Dastan, 2006). There have been other experiments performed using X-rays to obtain saturation profiles by direct measurements. In those experiments the core, usually Berea Sandstone but also Diatomite, is of known absolute or relative permeability and porosity. The core holder, that encloses the material is placed in an X-ray CT scanner, is non-metallic, for instance made out of plastic (PEEK, Ultem) or acrylic material (Dastan, 2006; Horne et al., 2000; Schembre & Kavscek, 2003). One experiment has been done on a gathering pipe at Svartsengi geothermal power plant using the same X-ray equipment as used in this project. In that project the aim was to map out slug flow in the gathering pipes and video was made of the two-phase flow by setting the equipment up so the side of the flow was visible. Because of the thickness of the steel the videos are not very good but sometimes some pulses of water flow could be seen (Á. E. Lund & Þráinsson, 2003).

## 1.2 Project goals and objectives

In this project, ways to measure saturation of water in steel pipes are explored both with and without gravel, the results can be applied in the Ph.D. project as previously mentioned. Finding ways to detect and quantify water saturation in the experimental apparatus used in the



Ph.D. project will be an added value to that project. Being able to quantify water saturation in the pipe while experimenting at high pressure is very valuable because then the processes inside the pressured pipe could be determined more accurately, in particular to quantify the relative permeability in two phase flow.

Main tasks of this project are:

1. Find out if detecting and quantifying water in steel pipes is possible with X-ray equipment available in the Biomedical engineering lab of Reykjavík University.
2. If task number 1 is possible, then set up experiments with steel pipes and use the X-ray equipment to detect and quantify water saturation in steel pipes. Both as the only component and also mixed with rock material and then process the data from those experiments.
3. Find out if Neutron meter that is used in borehole logging can be used to detect and quantify water in steel pipes.

These tasks were performed at the Reykjavik University using the existing X-ray equipment. Steel pipes were gathered for the project and prepared for the experiments in the machine shop at Reykjavik University.

## **2 Theoretical background**

### **2.1 X-rays**

X-rays were first discovered in 1895 by Wilhelm Konrad Röntgen (Röntgen, 1896) and like in many other experiments he got something more from his experiment than he expected. Röntgen had been experimenting with cathode ray tubes using fluorescent screens, (cathode ray = beam of electrons). He observed that something was emitted from the tube causing the fluorescent screen to glow. This happened even while the tube was in a closed box, so he soon realized that the tube he was experimenting with was not only emitting visible light but a new kind of radiation as well. This new radiation could not only travel through the box that enclosed the tube, but other material as well. He found out that the radiation was attenuated by various materials in different ways and that it could be captured on a photographic plate, like light. Because of the mysterious nature of the radiation, Röntgen decided to call it “X-ray” (Röntgen, 1896). Relatively short after Röntgen’s discovery the first “Röntgen image” of a hand was made and radiographs were commonly used in clinical practice short after that (Suetens, 2009, p. 14).

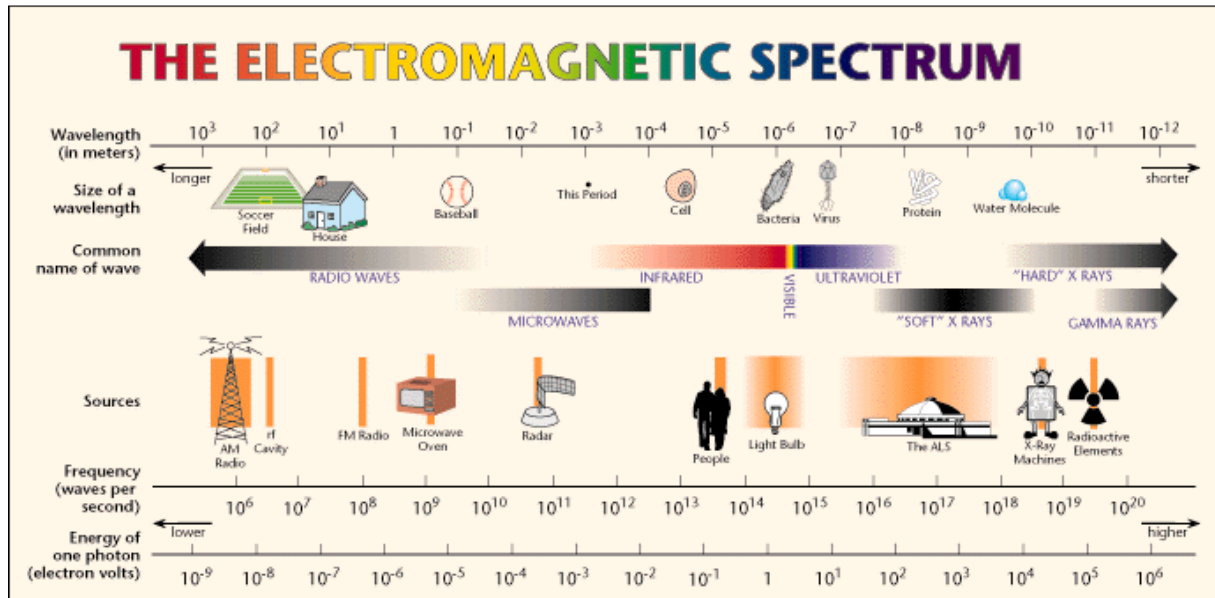


Figure 4: Spectrum of electromagnetic radiation (Berkeley lab, n.d.).

X-rays are electromagnetic waves that consist of energetic photons. The electromagnetic spectrum is divided into bands according to the wavelength and can be seen in Figure 4. The longest wavelengths are the radio waves, then there are micro waves, infrared, visible light, ultraviolet light, X- rays and gamma rays have the shortest wavelength.

Photon with the wavelength  $\lambda$  , frequency  $f$  , has the energy  $E$  as described in Eq. (1):

$$E = hf = \frac{hc}{\lambda} \quad (4)$$

$h$  is the Planck's constant and  $c$  is speed of light in vacuum. The wavelength of X-rays is usually measured in Ångström ( $10^{-10}$  m) and the photon energy in keV ( $1\text{eV} = 1.602 \cdot 10^{-19} \text{ J}$  ).

As stated earlier the X-rays are generated in a tube, called X-ray tube, which consists of a vacuum tube, a cathode and an anode and can be seen in Figure 5.

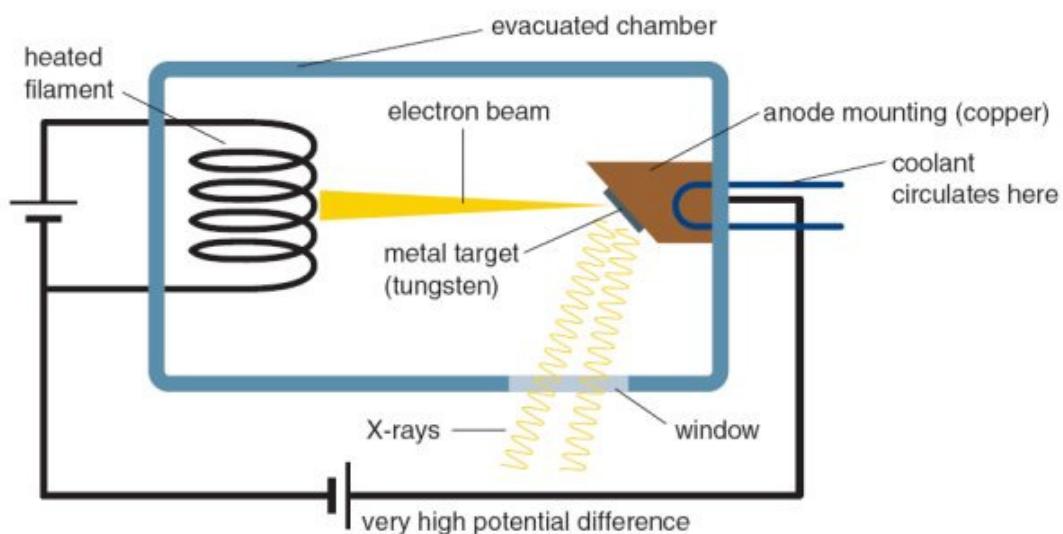


Figure 5: Schematic of an X-ray tube (Simmons, n.d.)

Electrons are released from the cathode by thermal excitation. The voltage between the cathode and the anode accelerates the electrons toward the anode.

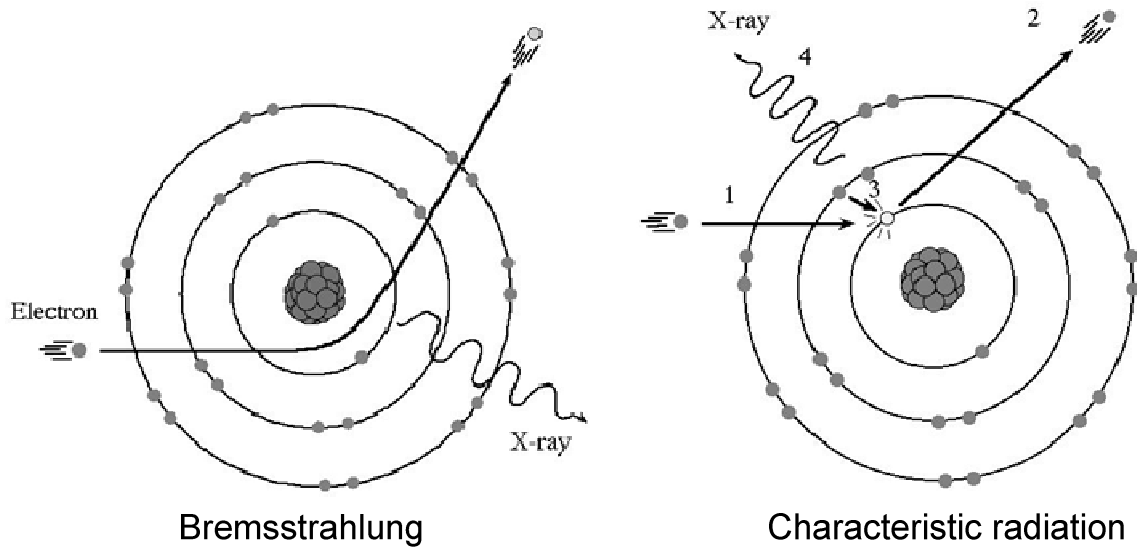


Figure 6: Bremsstrahlung and Characteristic radiation (*CT physics, 2006*).

When the electrons hit the anode and decelerate, they can release some, or all, of their energy and some of it is released as X-rays (about 1% of the initial kinetic energy) as bremsstrahlung and characteristic radiation. Bremsstrahlung has a continuous energy spectrum; the electrons that go near a nucleus and are slowed down form photons in the process, the closer they get to the nucleus the more energy is carried by the emitted photon. Characteristic radiation is when a fast moving electron clashes with an orbital electron exciting it to a higher energy level or even ejecting it from the atom, thereby leaving a “hole” at a low energy state (see Figure 6). That hole is then refilled with an electron from a higher energy shell which emits a photon of a specific energy which is the difference in energy of the two electron states. If an electron from the L-shell falls “down” to K-shell then the energy of the emitted photon is equal to the energy drop (difference):

$$E = E_L - E_K \quad (5)$$

A photon of this particular energy is emitted and yields the characteristic peaks in the X-ray energy spectrum (Suetens, 2009). The energy spectrum of an X-ray beam can be seen in Figure 7.

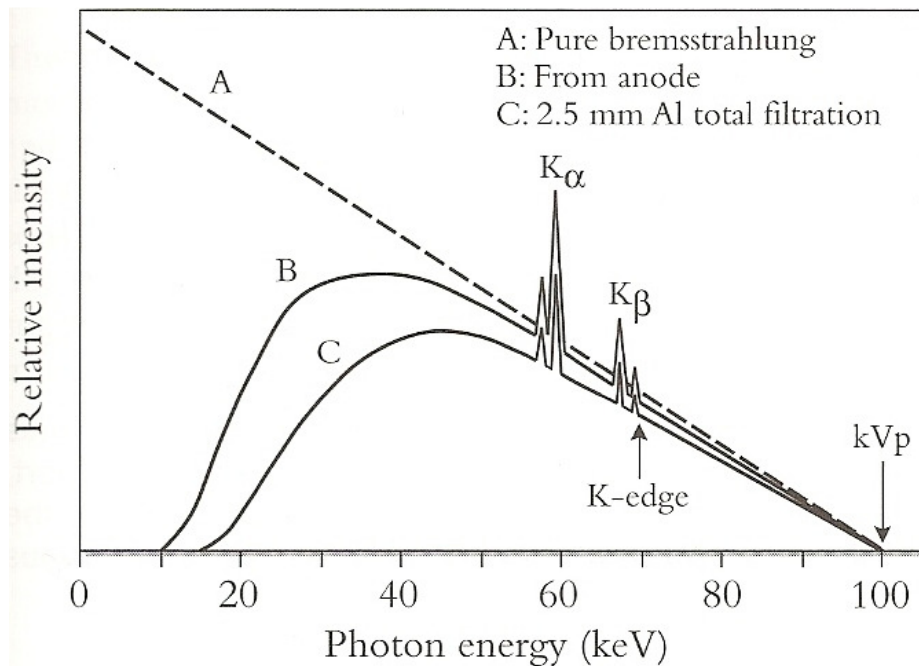


Figure 7: Energy spectrum of an x-ray beam generated in an X-ray tube,  $K_\alpha$  and  $K_\beta$  are due to L-shell and M-shell drops respectively (Wolbarst, 2005, p. 301)

Important parameters of an X-ray source (i.e. X-ray tube):

- The amount of electrons that hit the anode in the cathode tube and then the amount of emitted photons are controlled by the cathode current (often measured in mA) and by the time the current is on. Typical values are 1 to 100mA s for simple medical imaging.
- The energy of the electrons hitting the anode and subsequently, the energy of the photons that are emitted, is controlled by the voltage difference between the cathode and the anode. Typical values for most medical examination is between 50 to 125kV excluding mammography when it is usually between 22-34 kV. The upper limit of the photon energy is defined by the peak voltage across the X-ray tube.

At the anode, the total incident energy (typically expressed in J) is defined by the voltage, the cathode current and the current running time  $1J = 1kV \text{ mA s}$ ). It has to be taken into account that usually a tiny portion of that energy is converted into usable X-rays or about 1%, the rest is degraded to heat within the anode in the tube (Suetens, 2009, p. 16).

## 2.2 Interaction with matter

### 2.2.1 Interaction mechanism

X-rays and  $\gamma$ -rays are ionizing, which means that such photons are able to eject an electron from an atom and thereby ionizing it. If the photons have less energy than 13.6eV (Suetens, 2009) they are non-ionizing and are not able to eject an electron from an atom, but in a

process called excitation they are able to raise the electron to a higher energy shell. Photons that are ionizing can interact with matter in different ways as can be seen in Figure 8.

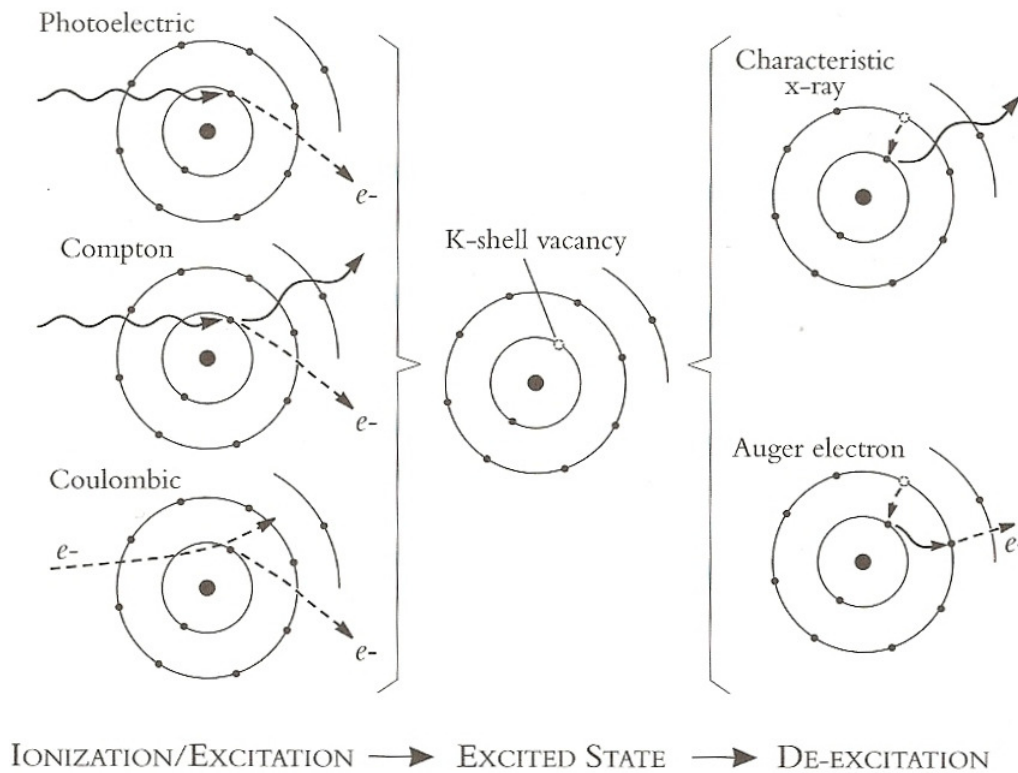


Figure 8: Interactions of x-ray with matter (Wolbarst, 2005, p. 91).

For our purposes the main ones are: Rayleigh scattering, Photoelectric scattering and Compton scattering. Rayleigh scattering (coherent scattering) is non-ionizing process that happens when the energy of the photons are low. This scattering occurs when the energy of X-ray photons is absorbed by an atom and emitted again as a new photon, travelling in different direction but with no change in energy. The scattering angle increases with decreasing energy. This interaction can be neglected in most radiological examination with peak voltage up to 125kV because these low energy photons are filtered out of the beam. For mammography the voltage is lower or 22-34 kV so Rayleigh scatter cannot be neglected. The second interaction is called Photoelectric effect. There, an incoming photon is completely captured by the atom, normally causing it to emit an electron. At still higher energies, interaction called Compton scattering, may occur. Then only part of the photon energy is used to eject an electron. A photon with the remaining energy is then emitted and its path deviates from the incoming photon. At still higher photon energy, at least 1.02 MeV, the incoming photon can transform into a positron and an electron - that mechanism is called pair-production. Positron has the same mass as the electron but opposite charge (antiparticle). When the positron will meet another electron, soon after it was formed, they will combine, making two photons that go off in opposite directions. Because of the high energy this occurs

in nuclear medicine and the photons can even cause nuclear reactions, but that is not used in medical applications (Suetens, 2009, p. 16). In Figure 9 is a graph showing the absorption probability of photons travelling through water for different photon energies and the range where different interaction mechanisms are relevant.

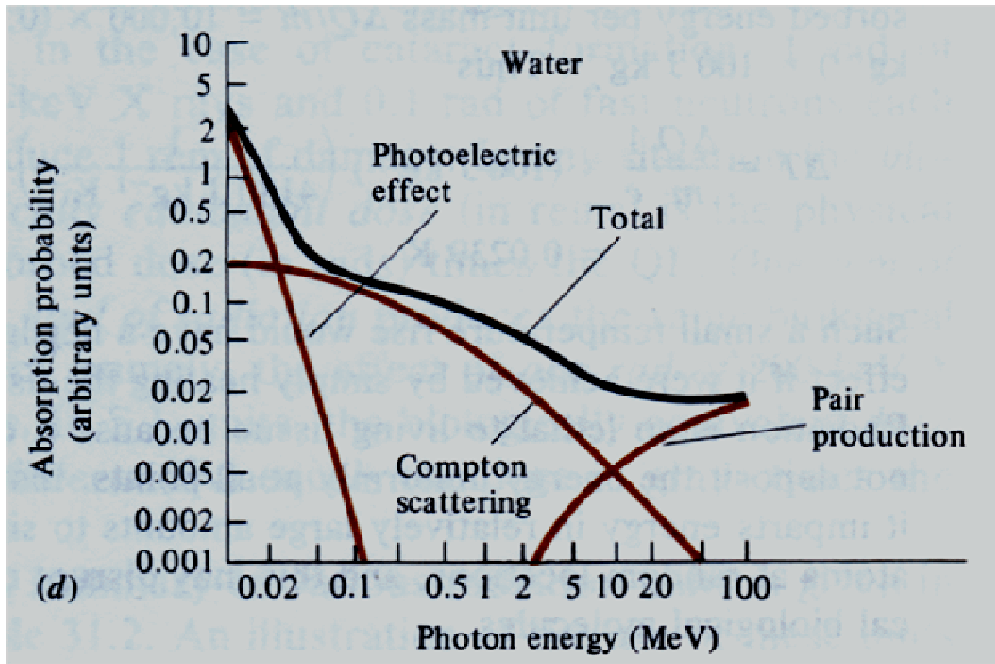


Figure 9: Absorption probability of photons while travelling through water for different photon energies (Sternheim & Kane, 1991, p. 829).

### 2.2.2 Interaction of X-ray with matter and rate of attenuation

Consider a block of material as in Figure 10,  $d = x_{out} - x_{in}$ . The X-ray beam is attenuated while it travels through the block by the interactions that have been described earlier. The connection between outgoing ( $I_{out}$ ) and incoming ( $I_{in}$ ) beam intensities are related by:

$$I_{out} = I_{in} e^{-\mu d} \quad (6)$$

Where  $\mu$  is the linear attenuation coefficient which is typically expressed in  $[cm^{-1}]$ .  $\mu$  depends on the photon energy, the density of the material and composition. This equation is only valid in a homogeneous material and when the beam consists of single energy photons.

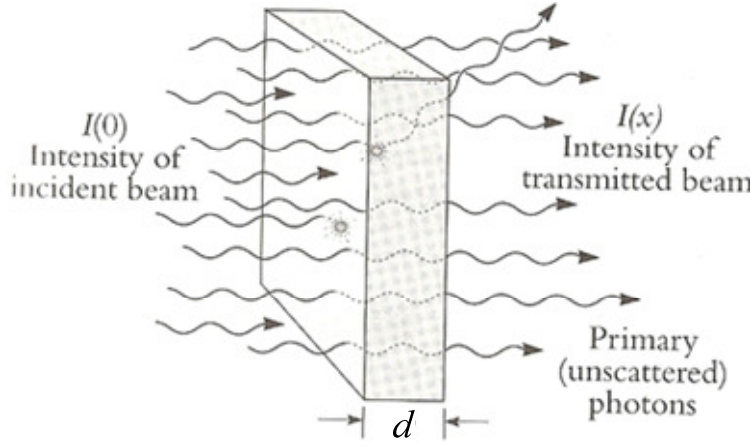


Figure 10: Travelling of an x-ray beam through a slab (Wolbarst, 2005, p. 153).

If the beam consists of single energy photons and travels through a medium that is non-homogeneous then the relation between  $I_{out}$  and  $I_{in}$  is:

$$I_{out} = I_{in} e^{-\int_{x_{in}}^{x_{out}} \mu(x) dx} \quad (7)$$

A single photon energy X-ray beam is not common because real X-ray beam has a continuous spectrum of energy which consists of both characteristic radiation and bremsstrahlung. If the energy of the photons in the incoming beam is a function of the energy, such that

$I_{in} = \int_0^{\infty} \sigma(E) dE$ , then the intensity of the beam going out is then:

$$I_{out} = \int_0^{\infty} \sigma(E) e^{-\int_{x_{in}}^{x_{out}} \mu(E,x) dx} dE \quad (8)$$

Instead of the linear attenuation coefficient  $\mu$  one often uses the mass attenuation coefficient

$\mu_m$ :

$$\mu_m = \mu / \rho \quad (9)$$

Where  $\rho$  is mass density of the attenuating medium. As can be seen in Table 1, the attenuation is highest in Iron and the mass attenuation is similar for all the materials at higher energies. The linear attenuation of the materials is very different, mostly because of a very different density of the materials. For example the linear attenuation of air can be ignored for high energy X-ray beam.

**Table 1: Mass attenuation coefficients and linear attenuation coefficients for a few materials at four different energies (Siegbahn, 1955).**

	Mass attenuation [ $\text{cm}^2/\text{g}$ ]				Density [ $\text{g}/\text{cm}^3$ ]	Linear attenuation [ $\text{cm}^{-1}$ ]			
	50 keV	80 keV	100 keV	150 keV		50 keV	80 keV	100 keV	150 keV
Air	0,20	0,17	0,16	0,14	1,22E-03	2,48E-04	2,03E-04	1,89E-04	1,66E-04
Water	0,22	0,18	0,17	0,15	1,00	0,22	0,18	0,17	0,15
Iron	1,90	0,59	0,37	0,20	7,87	14,95	4,64	2,91	1,574
Concrete	0,35	0,20	0,17	0,14	2,40	0,84	0,48	0,41	0,336
Glass	0,302	0,189	0,166	0,139	2,23	0,67	0,42	0,37	0,310

As can be seen in Figure 11, only a small fraction of the photons make it, unaffected all the way through the test subject which is mostly the result of the high attenuation of Iron (steel). Just going through 4,5 mm of steel the photons go down to 14% of their original number.

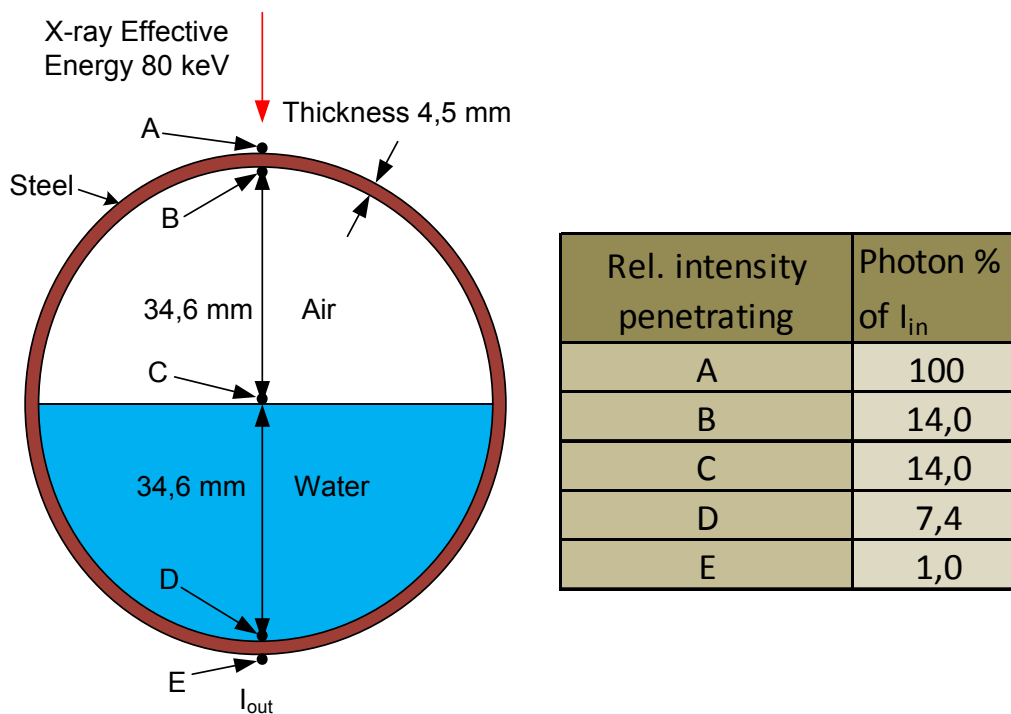


**Figure 11: Cross section of pipe nr. 4 (see chapter 4.4) and the results of calculations of the beam intensity through the pipe for at the effective energy calculated at page 27.**

## 2.3 Neutron logs

Neutron logs have been used for decades in well logging. Shortly after World War II the first neutron device appeared and the initial application was to determine formation porosity or to obtain an estimate of formation porosity (Ellis & Singer, 2008). Conventional neutron porosity logging tool is relatively simple, consisting of a neutron source and a detector or two. Even though the output of the logging device is often labelled “porosity” it is not quite as simple as that. The response from the logging tool can be described best by the slowing down length and where thermal device is the case the formation macroscopic thermal neutron absorption cross section, and the symbol for that is  $\Sigma$ . The slowing down length is not an



intuitive parameter, even though it is a convenient summary of the neutron transport properties. Codes have been developed for computers to calculate its value from formation constituents. For some applications the slowing down length can be computed from two or more conventional formation parameters; the hydrogen weight fraction and the bulk density. The former parameter is very useful in comparing neutron porosity results with core analysis, usually in weight fractions or in interpreting shaly sands (Ellis, 1990).

The neutron logging device is a pipe that is usually over one meter long and has either one or two detectors (then called near and far detector as seen in Figure 12) and a source at the other end of the pipe.

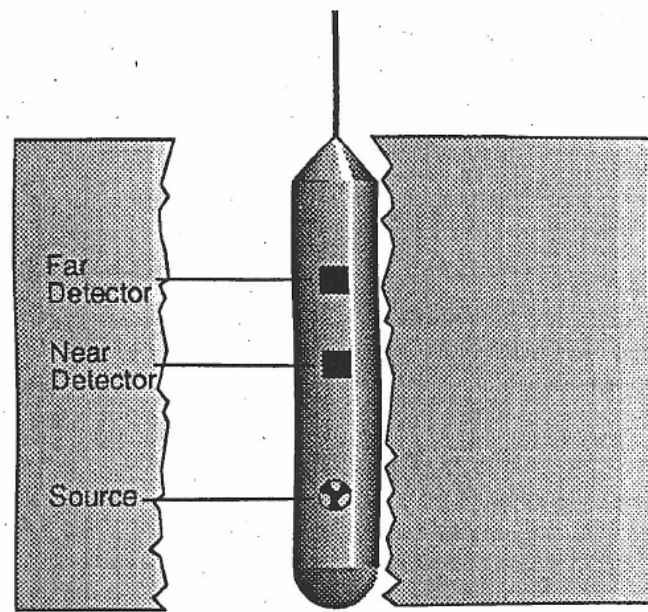


Figure 12: Neutron well logging device in a borehole, there is usually a bracket that presses the device up against the wall of the borehole so that it can obtain data from the strata the borehole goes through (Ellis, 1990).

Neutrons can interact with materials in different ways but here scattering will only be mentioned. Using neutron scattering to determine porosity is complicated due to the interactions of neutron with matter.

The elastic scattering of neutron with formation nuclei is the principal phenomenon that is exploited. The energy reduces, at each scattering depending on scattering angle and the mass of the scattering nucleus. Hydrogen mass is very close to the neutron mass and therefore it is very efficient in this energy reduction process and that is the principle that the measurement of the device is based on, the fact that hydrogen is very efficient in the slowing down of fast neutrons. When neutrons collide with hydrogen they can lose their entire energy in a single collision so that the number of collision necessary to reduce the nominal energy of neutrons in water is approximately 16 when it is 132 in a non-porous limestone (Ellis, 1990).

### 3 Experiment setup

#### 3.1 Steel pipes

The setup of the experiment started in May 2011 when a number of different steel pipes with different dimensions were collected and prepared. Table 2 summarizes the dimensions of these pipes, pipe nr. 6 in the table is of same material and dimensions as the pipe that is being used in the connected Ph.D. project which is mentioned in the Introduction.

Table 2: Pipes used in the experiments

Number of test subject	Outer diameter [mm]	Wall thickness [mm]	Inner diameter [mm]	Length [mm]
1	89,1	6,3	76,5	292
2	76,2	8,0	60,2	313
3	76,2	3,6	69,0	378
4	76,2	4,5	67,2	370
5	168,0	4,6	158,8	500
6	273,0	5,0	263,0	500

In the experiments, the pipes were installed so their axis was horizontal and water and rock material inserted into the pipes. To close the pipe ends, one end of the pipe was welded shut and tested to be waterproof and the other end was also closed to approximately half open by welding a piece of metal to it. This preparation can be seen in Figure 13.



Figure 13: Pipe with welded ends.

The pipes were prepared in that way so that water and rock material could easily be inserted into the pipes in the experiments. On later stages in the experiments, this half closed end was fully closed using Plexiglas fitted with a ruler as demonstrated in Figure 14 and a hole was drilled on the upward facing wall of the pipe as a water inlet. The material that was used in the experiment was inserted into the pipe and it then closed with the Plexiglas and water then added through the hole. The benefits of closing the pipe completely with Plexiglas are the possibilities of filling the pipe completely with water and seeing the water level through the Plexiglas. Figure 14 demonstrates this setup where the Plexiglas end can be seen and the water level in the pipe is also visible. The ruler is attached to quantify the water amount in the pipe.

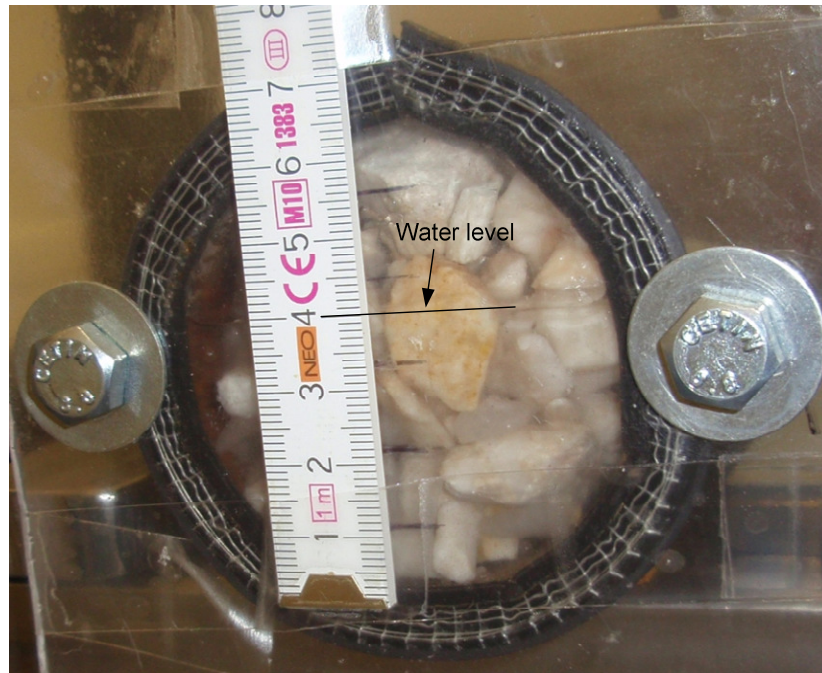


Figure 14: Pipe fitted with Plexiglas end with ruler attached.

### 3.2 Imaging equipment

The X-ray machine used in the experiments is a C-arm machine manufactured by Siemens in Germany 1988 owned by Reykjavík University and located at the Biomedical engineering laboratory. Figure 15 demonstrates the experimental setup for the x ray equipment in the laboratory at Reykjavik University where this experiment was performed.

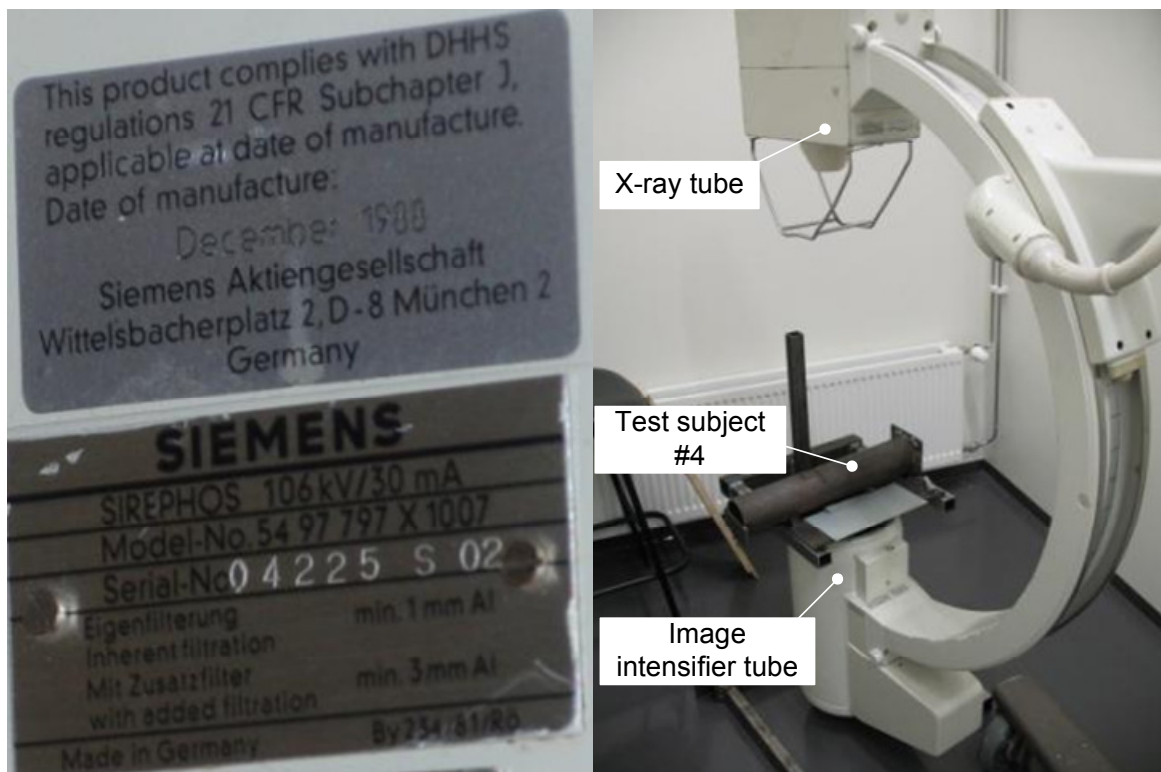


Figure 15: Photos of the X-ray machine and the experiment setup in the Biomedical engineering lab at Reykjavík University.



**Figure 16:** TV-screens that display the images from the X-ray machine.

As can be seen in Figure 15 the maximum attainable energy of the X-ray beam is 106 keV which is typical for this kind of medical equipment. The C-arm of the X-ray machine is very manoeuvrable so that machine is very good in that aspect. Operating this machine had some challenges because it has automatic image

enhancement built into it adjusting both the energy of the beam and the displayed image on the TV-screens seen in Figure 16. When the machine had been operated in automatic mode and was switched to manual mode, the adjustments that had been selected in the automatic mode, changed to a default setting resulting in a great change in the X-ray image, only by changing from Auto to Manual setting. The automatic setting was used mainly because using the manual setting was notoriously hard and the images from the machine often changed between experiments. Having the same energy in the X-ray beam allowed us to compare the images in a more realistic manner and that is why it was decided to have the X-ray images taken at the same energy level, highest output of the X-ray machine.

To get the machine to automatically go to the desired setting and to close the rest of the receiver that the pipe did not cover, there had to be good screening or sort of collimator around the pipe which was done with steel plates (see Figure 17). On one side there was 15 mm x 50 mm x 300 mm and on the other side was 8 mm x 100 mm x 300 mm. For adjustment 0,8 mm sheet metal plates could be added as needed, usually just one but could go up to three, and on the top of that the step wedge (see chapter 6) was placed.

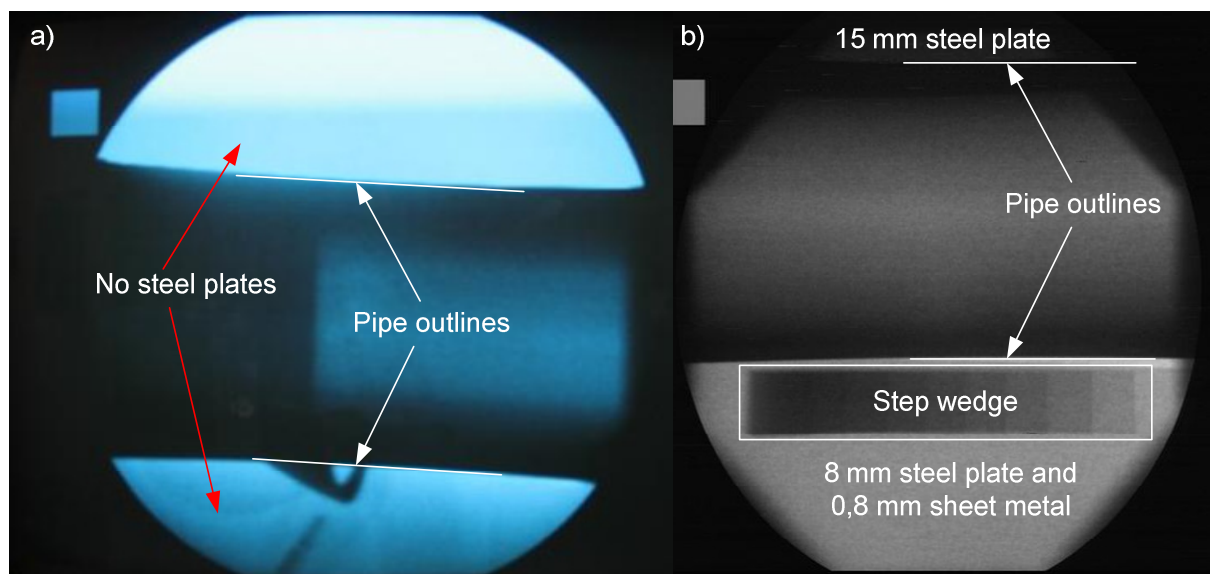


**Figure 17:** a) Image taken with no screening, b) Image taken with screening and a step wedge



In the first two experiments the X-ray machine was not connected directly to a computer for processing the X-ray images. The only way images could be transferred to a computer, was by taking digital photos of the screen of the X-ray machine with a digital camera and then load them onto the computer. After the first two experiments a cable and Analogue-Digital converter (ADC) was obtained so that a computer could connect to the analogue feed going to the screen of the X-ray machine. Then the images could go directly from the imaging equipment to the computer and the video ADC is ENMVG from Encore electronics (“Multimedia | USB Audio/Video Grabber,” n.d.). With that software, the feed from the X-ray machine is a video on the screen of the computer which images can be snapped from and saved on the computer after every exposure.

Throughout the experiments with the X-ray machine, suitable protective clothing was used (lead aprons) and preventive measure like standing far away and behind a corner of a wall while making X-ray images. At one experiment the equivalent dose was measured and the measurement device (Tracero T406) was placed 3,1 m from the X-ray tube and about 1 m from the floor. That placement was a little closer and not behind the corner of a wall than the step button for the X-ray equipment was placed. The results from that measurement show that the total dose for that session was  $1,3 \mu\text{Sv}$ , and the background dose rate was  $0 - 0,3 \mu\text{Sv/h}$  and  $23 \mu\text{Sv/h}$  while the X-ray tube was on for 3 – 4 s each image. The standard limit on effective dose is 50 mSv/y (Wolbarst, 2005, p. 572) so the measured radiation dose is well under the standard limit.

### 3.3 Step wedge

After the first experiment session there was some discussion about the next steps of the experiment and how it was possible to evaluate the thickness of the water in the pipes. The greyscale value of the images, region of interest (ROI), changed while water was added to the pipes so something was needed to use as a reference outside of the pipe. It was decided to make a step wedge made of steel to use as a reference and it had to be of several thicknesses so it could span many values of greyscale in the X-ray images. At first it was made with four little pieces of sheet metal (ca.  $4 \text{ cm}^2$  each) that was 1 mm thick and stacked so that they overlapped and formed a 4 mm stack at the thickest and 1mm where it was thinnest. This was positioned on the side of the pipe that had the thinner screening (8 mm, the 0,8 mm sheet metal was added later in the experiments). First version of a step wedge was with 5 steps but the step area was found to be too small in the image processing so two pieces of metal, each equal to the first version in size were also milled by the author in the machine shop at

Reykjavík University and can be seen in Figure 18. The second version had combined 6 steps with 1mm difference between steps but the step area was still a little small so few units of greyscale could be measured.

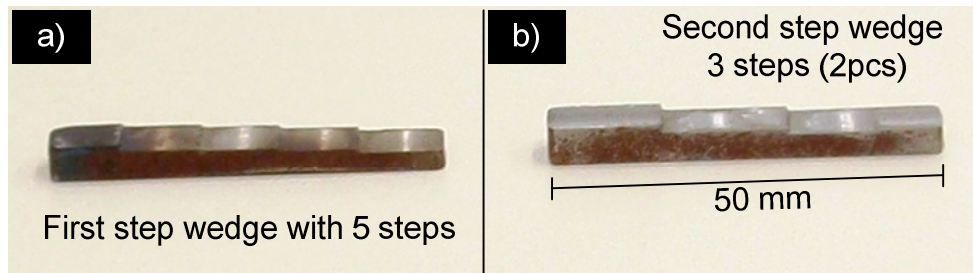


Figure 18: Photo of step wedges, a) First version b) Second version.

Then a new idea regarding sheet metal came to light and a new step wedge was made with 0,8 mm sheet metal that has 9 steps and can be seen in Figure 19.

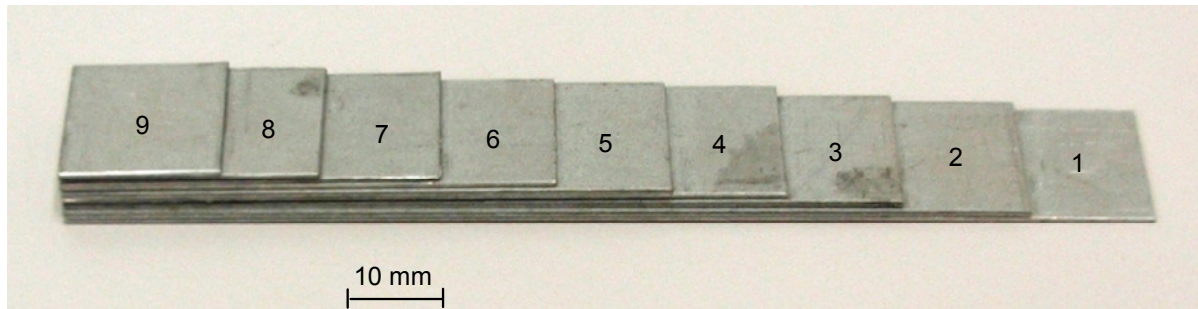


Figure 19: Step wedge, final version made with sheet metal, 9 steps 0.8mm each.

That was the final edition of the step wedge and was used in all the experiments that included rock material and water inside the pipes, the other step wedges from Figure 18 were only used in preliminary experiments with water. The step wedge has the function of being a scale that is the same throughout the experiments and is used as reference when measuring the greyscale and therefore the attenuation of the X-rays in the images as described in the next section.

### 3.4 Image processing

After getting the images from the X-ray equipment into a computer they were processed using the program ImageJ, which is image processing and analysis software. This program is widely used for technical purposes and can be downloaded free of charge from the internet at the URL: <http://rsbweb.nih.gov/ij/download.html>. With this program it is easy to obtain and manipulate the image value, the greyscale in a region of interest (ROI) in the images, as a number between 0 and 255 which is normal range in 8 bit greyscale image. In the images in this experiment the greyscale value for black is 0 and consequently the value for white is 255. In Figure 20 shown how the data was obtained from the images using ImageJ, region of

interest (ROI) is selected, and ImageJ provides information on how many pixels are in that region, and their Mean, Min and Max values and standard deviation.

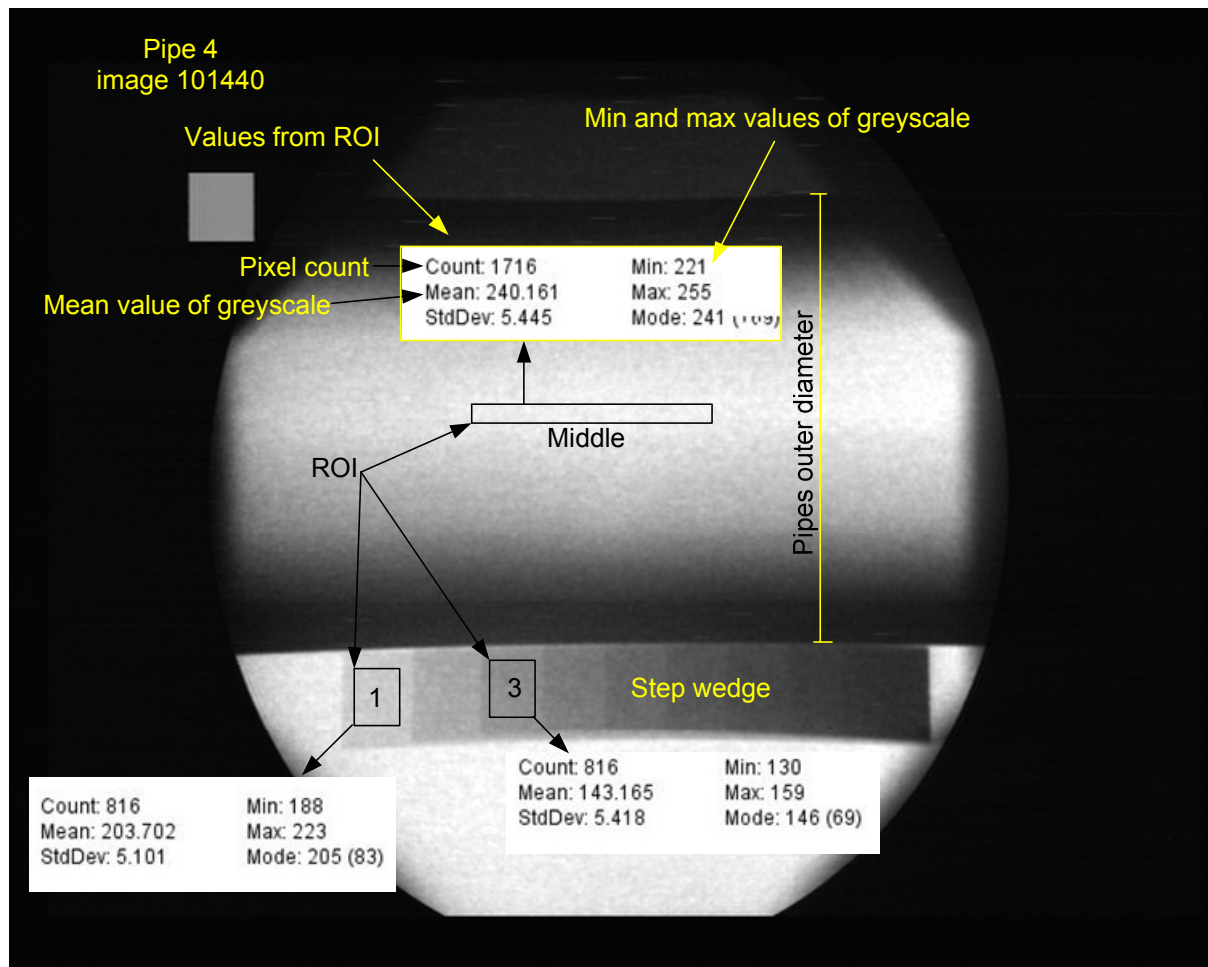


Figure 20: Demonstration of how the greyscale values are obtained for different regions in ImageJ.

### 3.5 Rack for the pipes and rock material

To be able to keep the pipes horizontal, a rack had to be built because even though the C-arm receiver can be horizontal it is not recommended to put the pipe directly onto the image intensifier tube. It also had to be sturdy enough to hold up the biggest pipe full of material and water. The rack was designed so that the pipe would have minimal clearance from the image intensifier tube and was made out of rectangular steel profiles in the machine shop at Reykjavík University.

The material used in the experiment was water, Quartz and Basalt gravel and the rock material can be seen in Figure 21. The Quartz was from Spain, obtained from a Ferrosilicon factory run by Elkem at Grundartangi. It was delivered in fist size nuggets which were too big to fit the small pipes so they were crushed down with a hammer by the author. The Basalt

gravel, 3-5 mm grains, was obtained from Björgun hf which is a company that sells many kinds of materials they get from seabed.

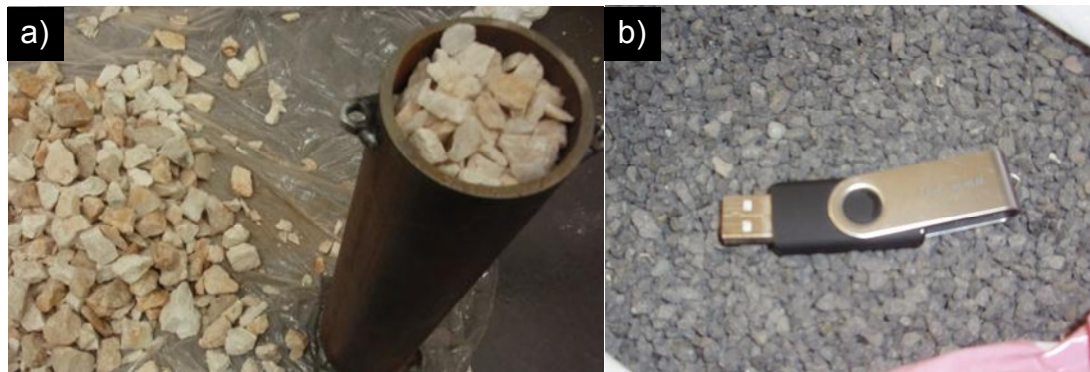


Figure 21: Photos of the material used in the experiments, a) Quartz ca. 5 – 30 mm and b) Basalt gravel 3 – 5 mm (memory stick for size comparison).

## 4 Measurements

A pilot study was performed in June 2011 which had the sole purpose of finding out if the X-ray equipment available in Reykjavik University was sufficient for the proposed experiments. The first few experiments were performed with the smaller pipes (nr. 1-4 in Table 1) because it was not clear in the beginning that using X-rays to quantify water in steel pipes was possible so we used the pipes that we had on site at first. Water was poured into the pipes so that the water level was in the vicinity of the middle of the receiver of the machine and a picture was generated as can be seen in Figure 22. That worked for all the pipes and the water level was very visible in them all except in pipe nr. 2 which had the greatest wall thickness of the four pipes, 8 mm. The next experiments were mostly made to improve the setup of the experiments and consequently the screening was added and a step wedge was made so that there was a reference point on the image outside the test subject.

After the first three experiments it was decided to acquire a piece of the pipe ( O.D. 273 mm) that is being used in a connected Ph.D. project mentioned in the Introduction and also a pipe with dimensions (O.D. 168 mm) in between the smaller pipes (O.D. 76,2 mm – 89,1 mm) and the pipe with O.D. 273 mm. The pipe numbers in the subsequent sections refer to Table 1 in Section 3.1.



#### 4.1 Pipe nr. 1

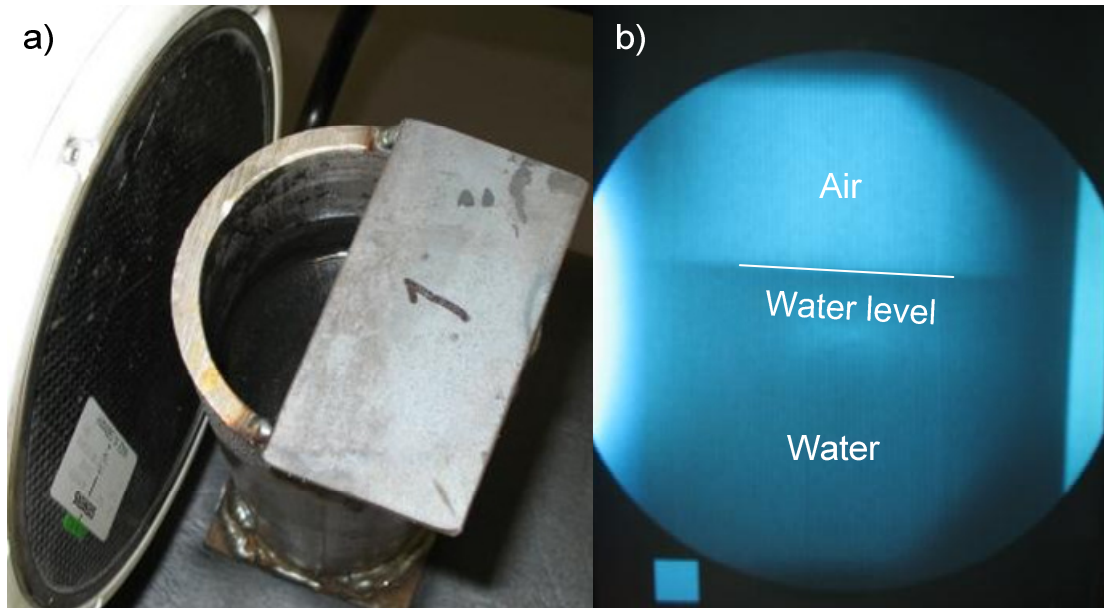


Figure 22: Photos from the pilot study with pipe nr. 1, a) Pipe nr. 1 near the image intensifier tube, b) Image from the X-ray machine.

When pipe nr. 1 (Figure 22) which has outer diameter of 89,1 mm and wall thickness of 6,3 mm, was first processed in a horizontal setup, it was gradually filled up with an increasing water level of 10 mm and an X-ray image taken at every step. When the images were processed in ImageJ the mean greyscale value obtained from the middle of the pipe when it was empty was 80,7 and when it was full of water 13,9 which is rather low. Numbers that low can be explained by the thickness of the steel in the pipe because the combined wall thickness is 12,6 mm. Adding rock material into this pipe will lower these numbers significantly and it is reasonable to say that the number will have reached 0 before the pipe is fully filled with water. In light of that information, experimenting with this pipe filled with rock material and then gradually filled again with water was abandoned.

In Figure 23 is a series of images from experimenting with pipe nr. 1, the pipe was not fully closed, as can be seen in Figure 22. The water level was not visible so the water that was poured into the pipe was measured, and the water height was calculated later which explains the intervals between the water heights.

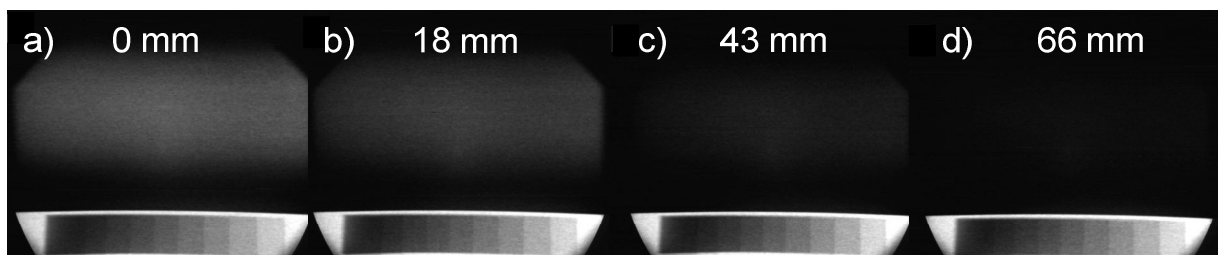


Figure 23: Series of images from experimenting with pipe nr. 1 OD 89,1 a) No water, b) Water height in pipe 18 mm, c) Water height 43 mm, d) Water height 66 mm.

## 4.2 Pipe nr. 2

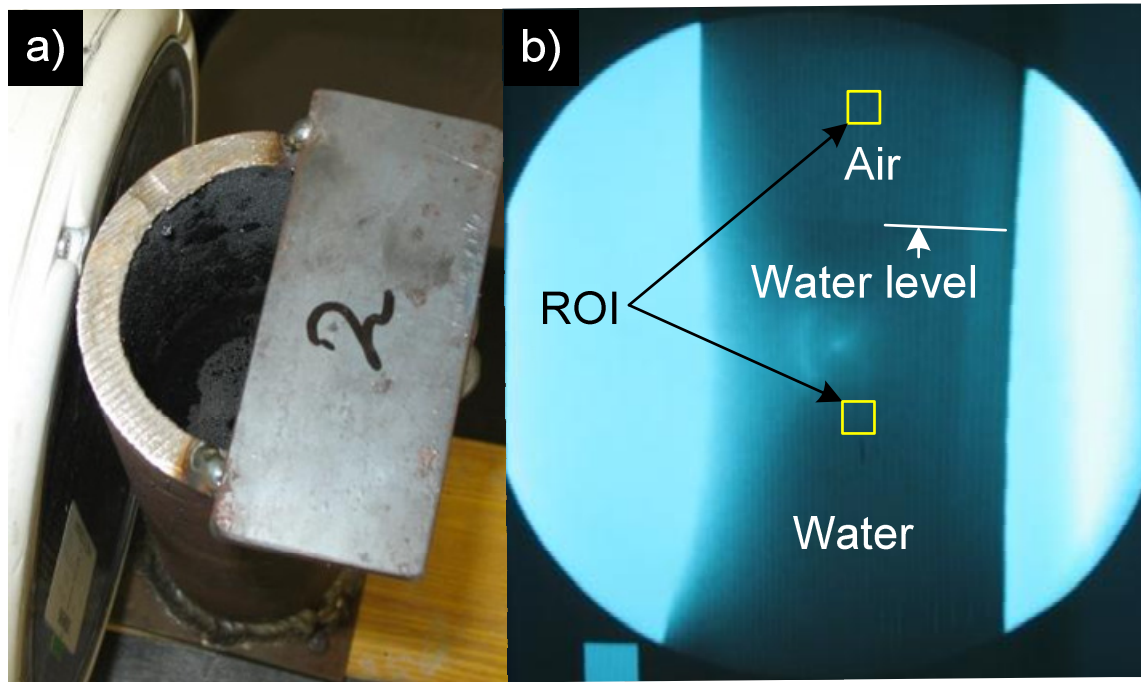


Figure 24: Images from the pilot study using pipe nr. 2, a) The setup, b) Image from the X-ray machine and the water level is barely visible.

Pipe nr. 2 (Figure 24 a), which has outer diameter of 76,2 mm and wall thickness of 8 mm, was the first pipe that was ruled out because the combined wall thickness is too great (16 mm). The purpose of the pilot study was only to see if water level could be detected in the pipes and there was some trouble at first just seeing the water level in this pipe. After doing some tricks like putting something on the pipe at the water level to mark the spot the water level could be detected. When the image (Figure 24 b) was processed in ImageJ the value of greyscale in region of interest (ROI) where water was filling the pipe was 67,33 and where there was no water the value was 68,55. The difference is 1,2 and because of that any further experiments on this pipe was discarded. The X-ray machine is obviously not powerful enough to penetrate steel this thick.

### 4.3 Pipe nr. 3

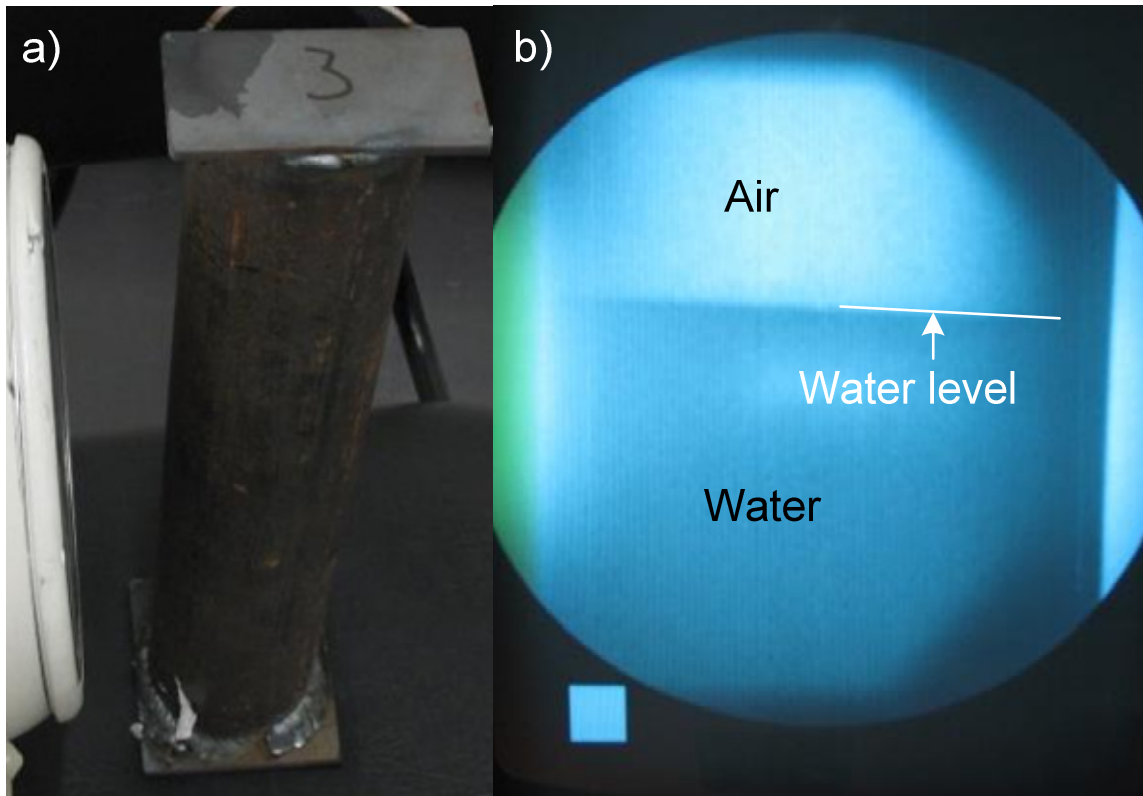


Figure 25: Photos from the pilot study with pipe nr. 3, a) The setup, b) Image from the X-ray machine showing that the water level is visible.

Pipe nr. 3 (Figure 25 a) which has outer diameter of 76,2 mm and has the smallest wall thickness of all the pipes or 3,6 mm. In the first experiment the water level was well detectable in this pipe as can be seen in Figure 25 b. When this pipe was tested in a horizontal setup with screening on both sides, the X-rays penetrated it very well and actually too well. The effect of that was that the automatic setting on the X-ray machine tuned the energy down for a better resulting picture. That means that when the pipe is filled with water and material, it was more difficult for the beam getting through and the energy of the X-ray beam is tuned up again when the aim is to have exactly the same setting throughout an experiment with a pipe. As it was not feasible to adjust the setting manually on the X-ray machine to obtain satisfactory images, there could not be an experiment using pipe nr. 3 with the same image setting throughout the experiment of this pipe. Therefore, experimenting further with this pipe using X-rays would not give comparable results.

#### 4.3.1 Neutron logging with pipe nr. 3

This pipe was also in an experiment with a Neutron meter at the Icelandic Geosurvey (ÍSOR) that did not give any result. The experimental setup for that is shown in Figure 26. That is believed to be due to the size of the pipe which cannot accommodate a lot of water and there

for not enough hydrogen which the neutrons act with and also the pipe itself is a hindrance for the neutrons.

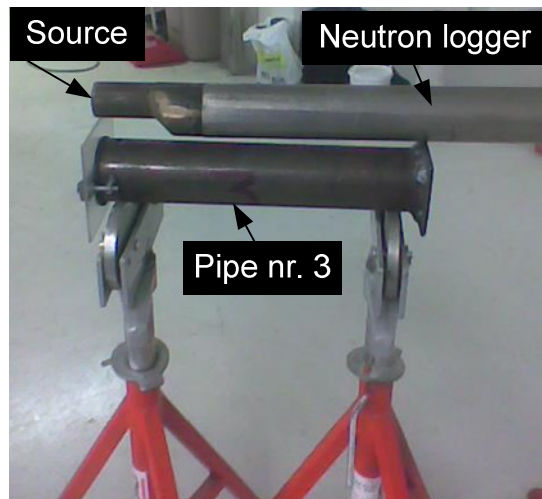


Figure 26: Pipe nr. 3 in a neutron logger experiment.

The reason pipe nr. 3 was chosen to be experimented on first in the neutron logger experiment was because the wall thickness of the pipe was the least of all the test subjects. This test was unsuccessful as the neutron logger did not show any results at any level of water in the pipe or it is not accurate enough for such a small amount of water in a small steel pipe.

#### 4.4 Pipe nr. 4

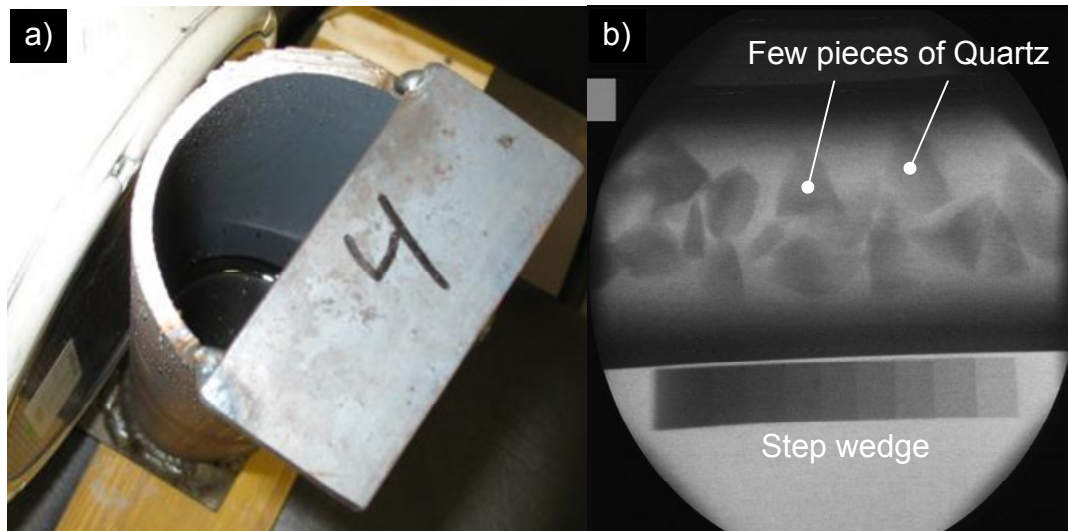
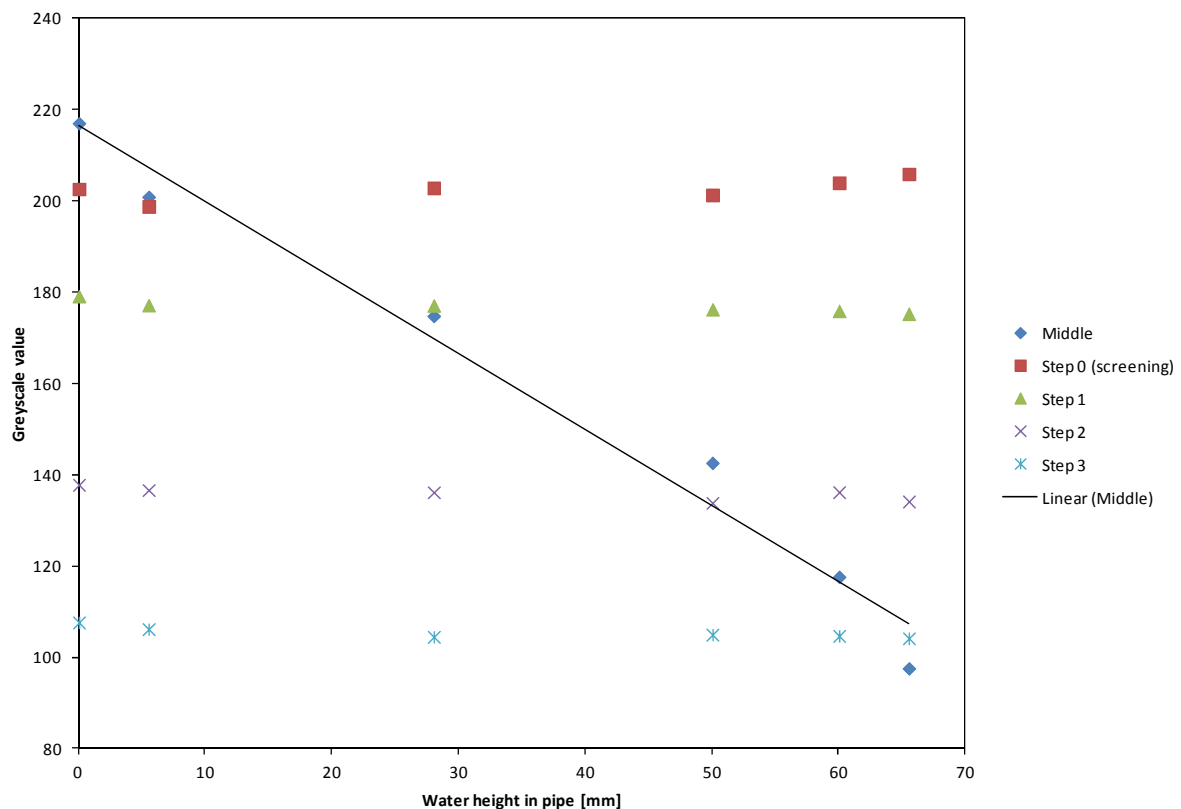


Figure 27: a) Image from the pilot study showing the setup, b) Image from preliminary experiment with few pieces of Quartz in the pipe.

Of all the pipes used in the experiments, pipe nr. 4 (Figure 27 a) which has the outer diameter of 76,2 mm and wall thickness of 4,5 mm, was the one that fitted the experimental setup best. When making the first image of this pipe while it was empty, the X-ray machine sometimes decreased the X-ray beam energy from the desired value of 106 keV. That means that this

pipe has just barely the total thickness of steel in its walls for the X-ray machine to maintain its most powerful setting. If the wall thickness was any less then getting X-ray images from this pipe would not have been quite as successful as it turned out to be.

Pipe nr. 4 was the only pipe that was fully tested throughout the experiments and was the pipe chosen when testing how the Quartz would turn out on X-ray image when a few pieces of Quartz were placed in the pipe as can be seen in Figure 27 b. The first process was filling it gradually with water making X-ray images at every step, then the water was poured out and the pipe filled with Quartz and the first process repeated and finally the Quartz was replaced with Basalt gravel and the first process repeated. The final experiments with this pipe were performed in November 2011 in the Biomedical engineering lab at Reykjavík University and the results can be seen in Figures 28-30. Figure 28 shows the results from the first process with pipe nr. 4 filling the pipe gradually with water and making X-ray images at every step.



**Figure 28: Results from experimenting with pipe nr. 4 filling it gradually with water and making X-ray images at every step at 106 keV and 6,4 mA.**

The difference between each step of the step wedge can clearly be seen in Figure 28 and for this experiment a greyscale value had to be obtained from the from the screening outside of the step wedge to go as low as the greyscale value for the empty pipe. The screening under the step wedge was 10,4 mm thick and consisted of 8 mm steel plate and 3 pieces of 0,8 mm sheet

metal, the same size as the 8 mm steel plate, made out of the same plate as the step wedge. The 2,4 mm of sheet metal was added under the step wedge while trying to adjust the automatic setting of the X-ray machine up to maximum setting at 106 keV. The highest greyscale value (217) is at the middle of the pipe while it is empty and is no surprise because there the steel that the photons in the X-ray beam travel through is thinnest, 9 mm. Greyscale value of 217 is quite high as the image is very luminous. The gap in the greyscale values between step 1 and 2 is hard to explain as there is the same difference of thickness in the step wedge so there should be a trend in the values for the step wedge. The greyscale values of the steps in the step wedge decrease with increasing thickness of the steel.

The water level is not at regular intervals which are resulting from pouring water into the pipe without measuring the water height. The height of the water level was calculated after this experiment from the volume of water poured in at each step. Data labelled “middle” is from ROI at the middle of the pipe where the water height is thickest at every step of the experiment. That ROI was chosen as it will provide the most difference in length of water looking at the side of the pipe and therefore the possibility of highest difference in greyscale. From the results in Figure 28 it can be derived that greyscale value measured for the thickness of 1 mm of steel in the step wedge is equal to 24 mm of water since the measured greyscale level follows the water level linearly. This was found by taking difference in water height values, between steps 0 – 3 giving 57,8 and divide that value with the thickness of the steel between the steps which is 2,4 mm.

The bulk attenuation (1mm in steel equivalent to 24 mm in water) indicates an effective energy of the X-ray beam is at approximately 80 keV, which is not unrealistic considering that the peak energy, of the energy spectrum used is 106 keV.

To find out the effective energy of the X-ray beam, Eq. 6 was used:

$$I_{out} = I_{in} e^{-\mu d} \quad (6)$$

If the attenuation is the same for steel and water then:

$$\begin{aligned} \frac{I_{out}}{I_{in}} &= e^{-\mu_w \cdot d_w} = e^{-\mu_s \cdot d_s} \\ -\mu_w \cdot d_w &= -\mu_s \cdot d_s \\ \frac{d_w}{d_s} &= \frac{\mu_s}{\mu_w} \end{aligned} \quad (6a)$$

Where  $d_w$  is the water height difference,  $d_s$  is the thickness of steel,  $\mu_w$  is attenuation of steel and  $\mu_s$  is the attenuation in the water.



To be able to calculate this, the attenuation for Iron and Water at different energies needed to be obtained and are the values for photon energy from 50 to 110 keV shown in Table 3.

**Table 3: Attenuation for Iron and Water at different energies.**

Photon En. [keV]	Iron $\mu$ [cm <sup>-1</sup> ]	Water $\mu$ [cm <sup>-1</sup> ]
50	15,7	0,232
60	9,9	0,213
70	6,8	0,196
80	4,4	0,184
90	3,6	0,179
100	2,9	0,173
110	2,7	0,167

The results from putting numbers into Eq. 6a show that the effective energy is 80 keV which is a bit high as the peak is 106 keV and compared to the energy spectrum in Figure 7. This can be the result of beam hardening, there is more of high energy photons left in the beam so the effective energy is higher.

In Figure 29 the results from experimenting with pipe nr. 4 full of Quartz material and gradually filling it with water are shown.

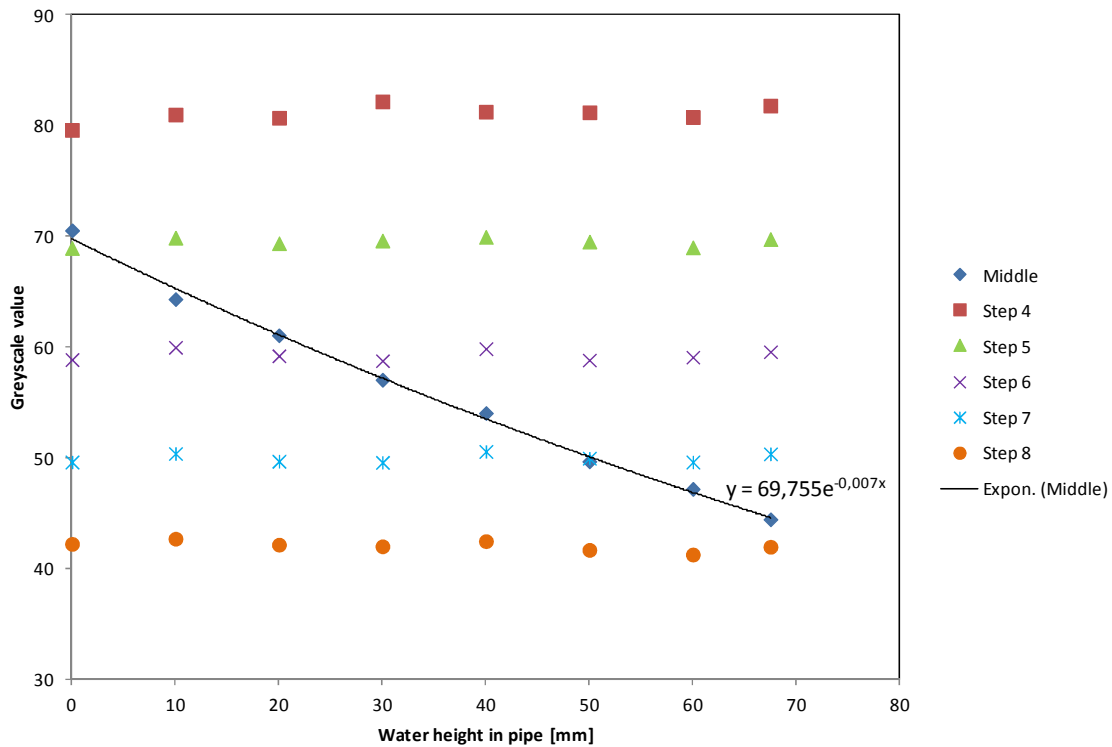


**Figure 29: Results from experimenting with pipe nr. 4 full of Quartz material and then filling it gradually with water and making X-ray images at every step at 106 keV and 6,4 mA.**

In Figure 30 are the results from experimenting with pipe nr. 4 filled with Basalt gravel and gradually filling it with water.

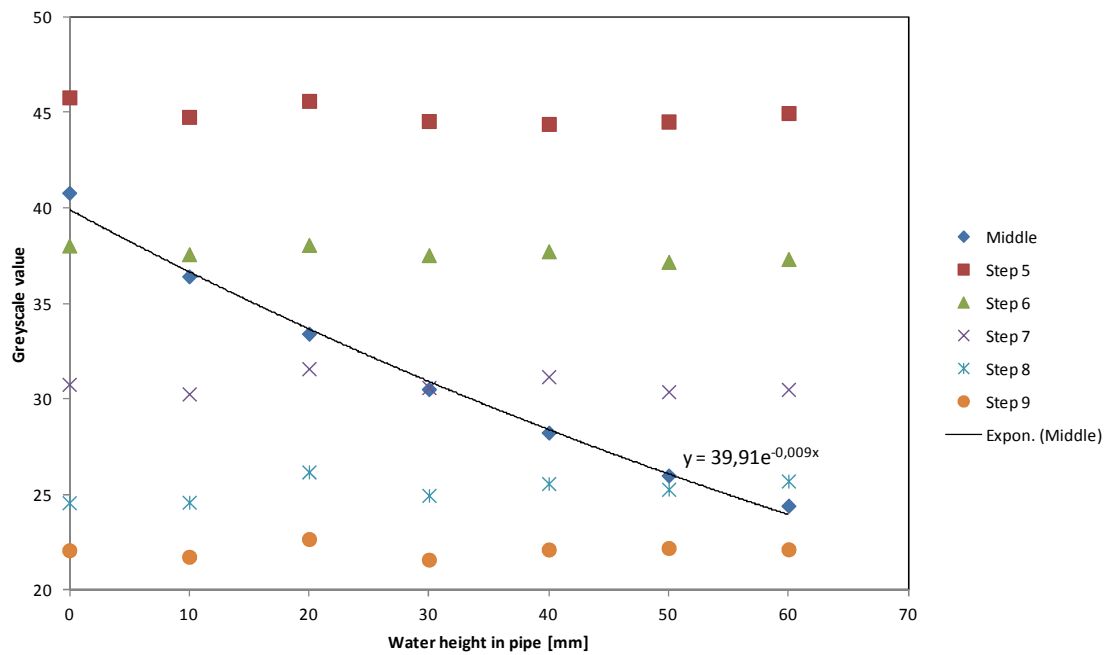


**Figure 30: Results from experimenting with pipe nr. 4 full of Basalt material and then filling it gradually with water and making X-ray images at every step at 106 keV and 6,4 mA.**

The Quartz attenuates the X-ray beam significantly as can be seen by comparing the greyscale values at water height 0 mm in Figures 28 and 29, the difference is  $217 - 70 = 147$ . The greyscale value for the “middle” is not only different as expected in Figures 28 and 29 but it is also spanning fewer values in the latter experiment shown in Figure 29 which is because the Quartz attenuates the X-ray beam more than air. As can be seen in Figures 29 and 30 the line that fitted best with the data was exponential but linear line is not very far from fitting also.

For the experiments with Quartz and Basalt, 1 mm of steel is the same as 30 mm of water in the pipe with Quartz material and 28 mm in the pipe with the Basalt material. Probably not a significant difference between Basalt and Quartz due to difference in volume, due to different grain sizes of the materials used. As expected there were higher number than for water alone because the water only fills part of the total volume due to the rock material.



#### 4.5 Pipe nr. 5

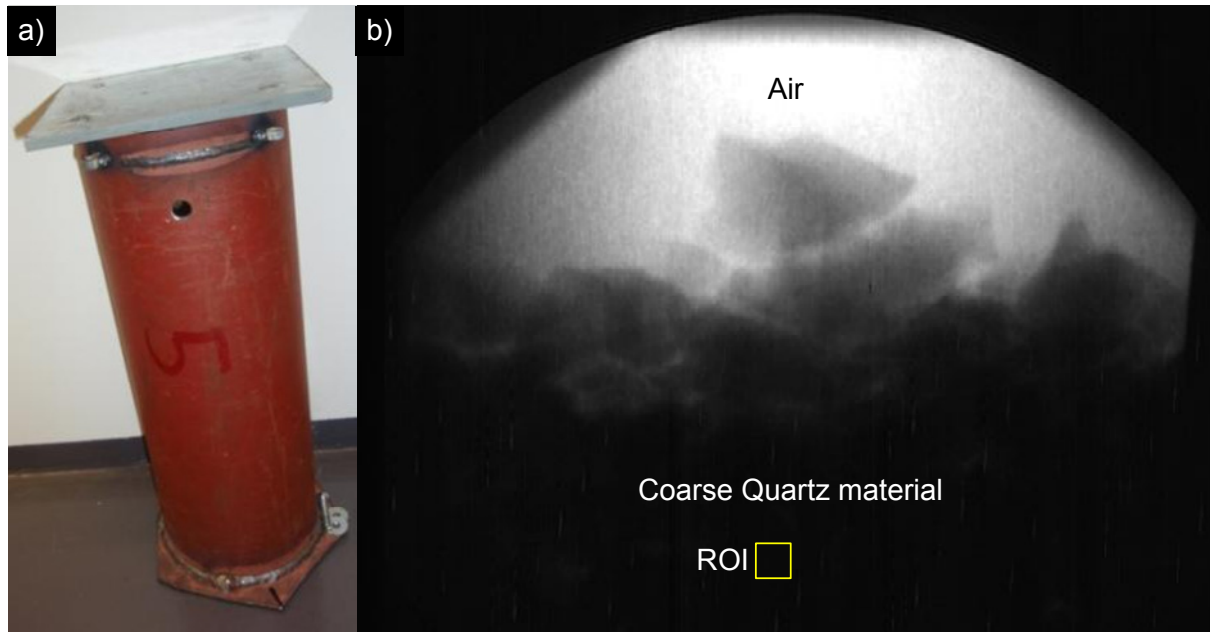
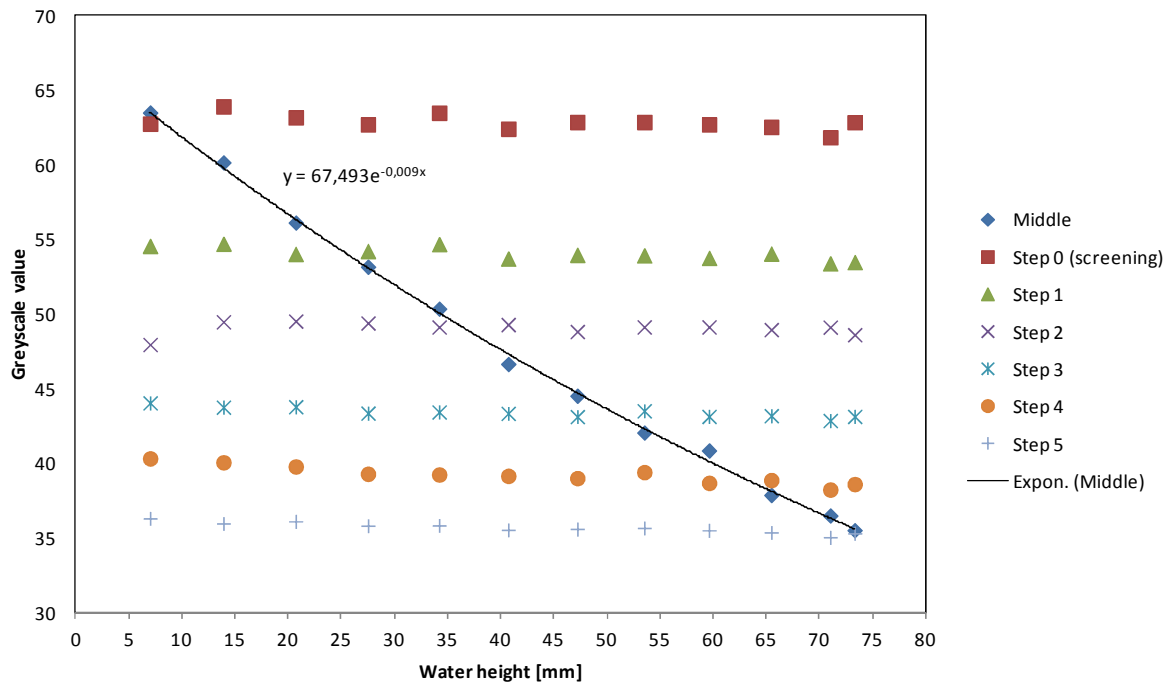


Figure 31: a) Pipe nr. 5, b) Image from the X-ray machine and the Quartz level is visible and but the X-rays did not penetrate the Quartz as needed and the greyscale value for the region of interest was only 14,5.

Pipe nr. 5, seen in Figure 31 a, is the second largest pipe with outer diameter of 168 mm and has almost the same wall thickness, 4,6 mm, as pipe nr. 4, which has wall thickness of 4,5 mm. The results of the first experiment that was made with pipe nr. 5 in a horizontal setup were very promising. That experiment was the first experiment made with a pipe horizontal on the rack while X-ray images were made as water was poured gradually into the pipe. The results from that experiment can be seen in Figure 32.

When the pipe was tested with Quartz material the energy of the X-ray beam was not sufficient to get any good result so further experiments with this pipe was abandoned. The image from that experiment can be seen in Figure 31 b) and as it says in the subtext of that figure the value for region of interest is 14,5 which is really low. That basically means that this pipe full of Quartz is nearly impossible to penetrate with the X-ray machine used in the experiments.



**Figure 32: Results from the first experiment with pipe nr. 5 filling it gradually with water and making X-ray images at every step at 106 keV and 6,4 mA, no rock material.**

Figure 32 is showing the results from the first experiment with pipe nr. 5, showing that the values for the steps are relatively the same throughout the experiment for each step which is a good sign of stability in the experiment. It also shows that as the water level rises, the values in the middle are reduced exponentially. In this experiment the pipe had welded ends and it was not possible to see the water level but the volume of water put into the pipe was documented and the water height was calculated after the experiment. There was actually a small error in the volume calculations that were not noticed until the experiment was over, so the water level is only about half of the diameter of the pipe at the end of the experiment.

The line is drawn linear through the data taken from the middle of the pipe where the water is thickest. A rough estimate was made from these results, a 1mm of steel is around 20 mm of water.

#### 4.6 Pipe nr. 6

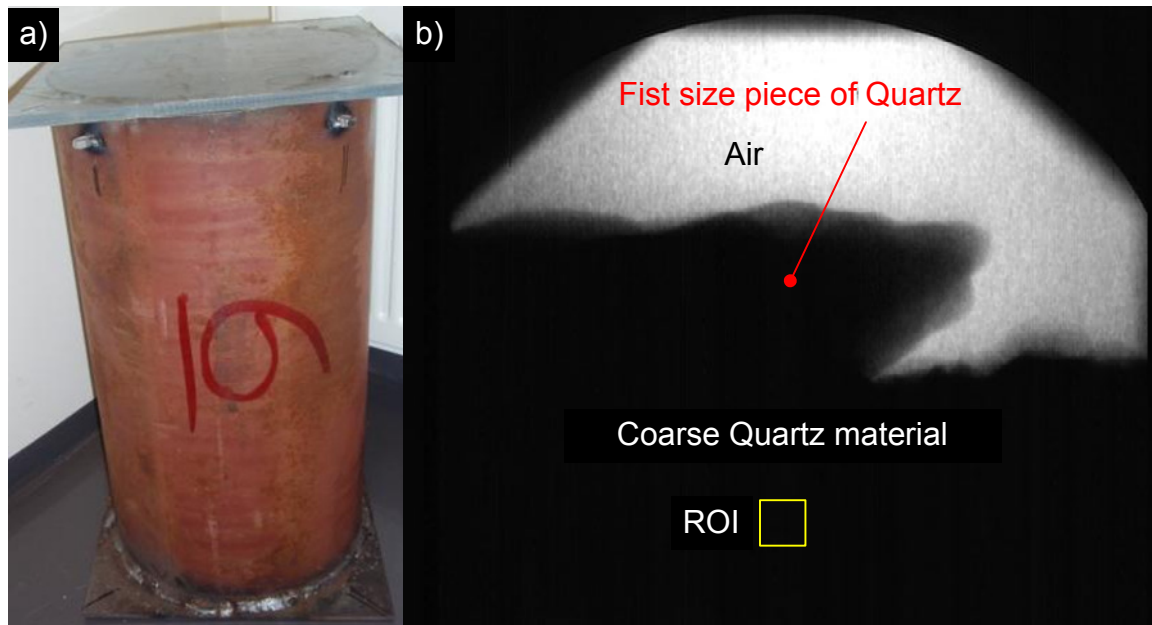


Figure 33: a) photo of pipe nr. 6 b) Image from the X-ray machine where the Quartz level is visible but the X-rays did not penetrate the cross section of the pipe filled with Quartz.

Pipe nr. 6 was a piece of pipe with the same dimensions as the pipe that is being used in the connected Ph.D. project and the biggest pipe, with outer diameter of 273 mm and wall thickness of 5 mm, was used in this experiment (Figure 33 a). This pipe is a lot bigger than the image intensifier tube which receives the X-ray beams. Therefore it is not possible to get the middle part of the pipe and the step wedge, outside of the pipe, into the same image as could be done while experimenting with all the other pipes. To get a good image of the cross section of this pipe, and the step wedge, it had been proposed to either to take an image of the

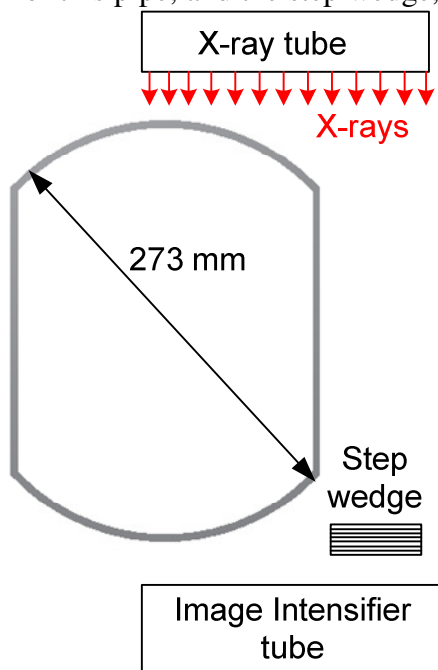


Figure 34: Schematic of how the diameter of pipe nr. 6 would have been changed to get image of the middle of the pipe.

end of the pipe were the step wedge could be at the side of the pipe or to weld plates into the pipe. By doing so the horizontal diameter would be smaller while the vertical diameter would keep its length. In that way the X-ray beam would have to go through the whole diameter as can be seen in Figure 34. After doing an experiment with the Quartz occupying the cross section of the pipe it was clear that the energy of the X-ray beam was not sufficient to penetrate cross section that large. Further experiment with X-rays with this pipe was then set aside and the focus put on pipe nr. 4.

#### 4.6.1 Neutron logging with pipe nr. 6

In December 2011 there was done an experiment on this pipe with a neutron logger at the facilities of Icelandic Geosurvey (ÍSOR) in Reykjavik. In this experiment, different setup was tested and two different neutron loggers. First neutron logger was from Gearhart-Owen with ca 15 cm long, single He3 neutron detector about 35 cm from the end where the source is attached. The second neutron logger was from Hotwell, dual detector also with He3 and the detectors are 37 cm and 67 cm from the end where the source is attached. Unlike pipe nr. 3, where nothing was detected, there was something going on in this experiment, the neutron logger detected the water but the specialists at ÍSOR have yet not identified what interactions took place (January 2012).

The steel in the pipe has definitely big effect on the results as can be seen in Figure 35 which is from a measurement by ÍSOR at a well that has a casing down to about 35 m depth.

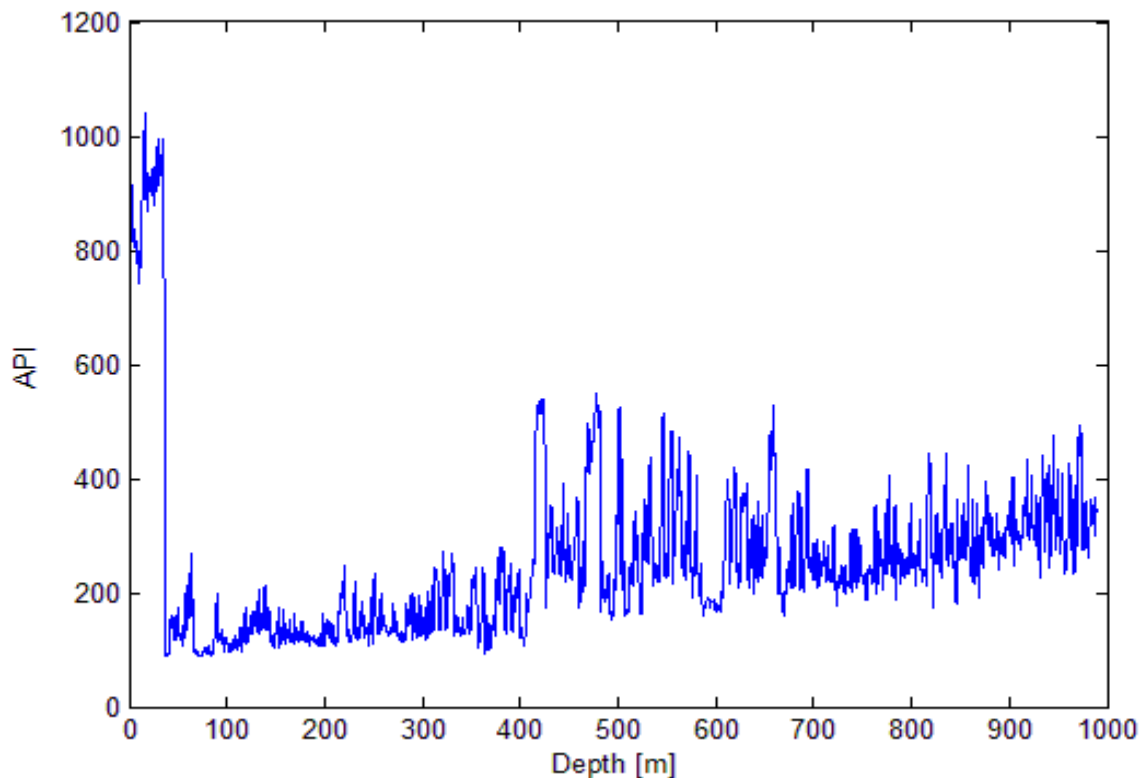


Figure 35: Results from a neutron logger at a well with casing to approximately 35 m depth.

As can be seen in Figure 35 the API value is much lower where there is no casing present.

These results are shown here to give an idea of what to expect from using the neutron logger in this experiment. Putting the neutron logger into a well where it is surrounded by the well is of course very different from putting it outside of a steel pipe where only a partial part of the circumference of the neutron logger is covered.

In Figure 36 are results from the experiments with neutron logger and pipe nr. 6 while filling it gradually with water and when it was full it was waited until equilibrium was reached and then the pipe was drained again.

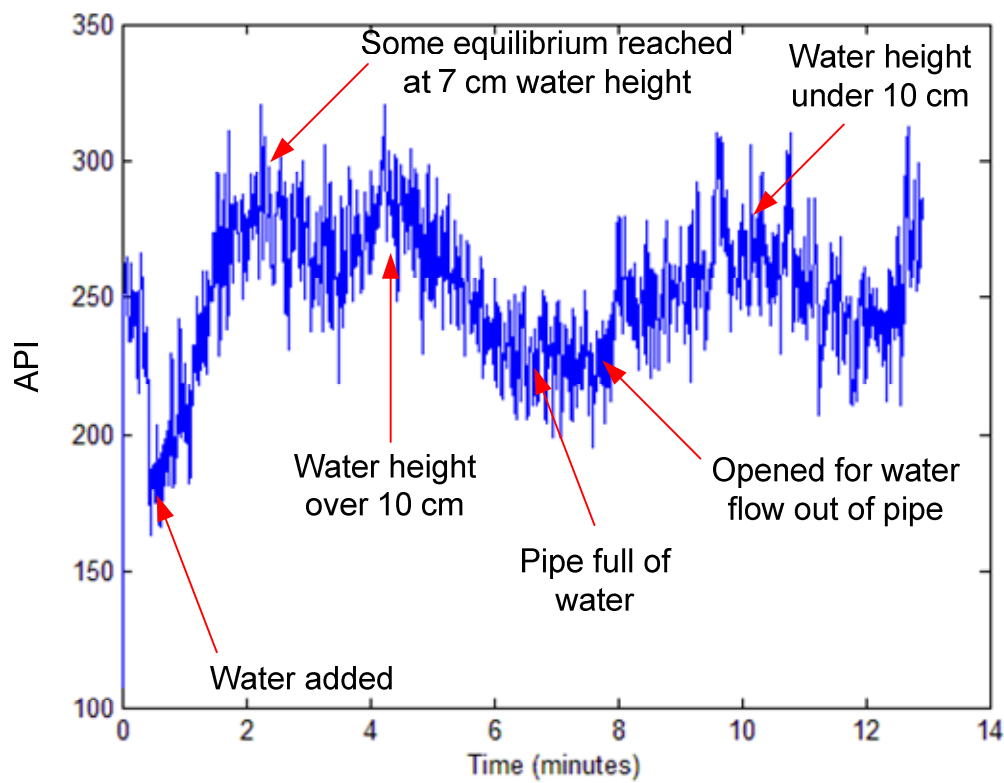


Figure 36: Results from experimenting with neutron logger and pipe nr 6 filling it gradually with water

The results from one of the experiments with the neutron logger and pipe nr. 6 can be seen in Figure 36. The expected behaviour was that the neutron count would go lower when water was added to the pipe but instead the count went higher until at certain level in the pipe and then it went down again until it was full. When the pipe was drained the same behaviour continued in reverse while the water was slowly going out of the pipe.

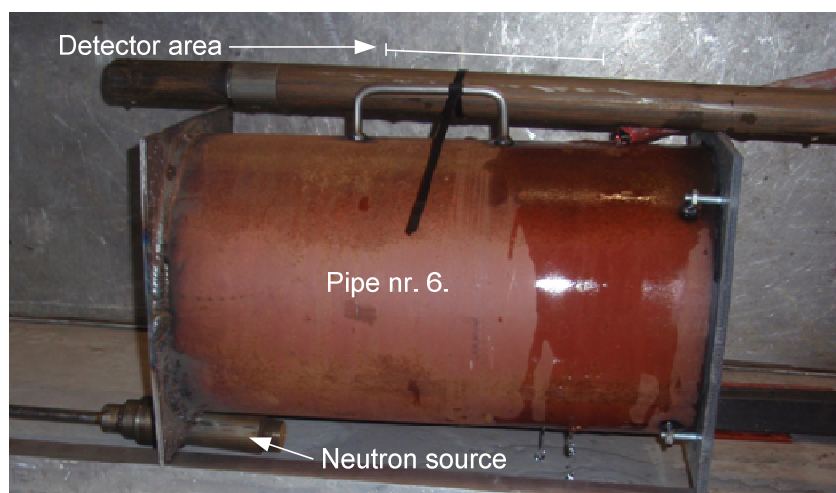
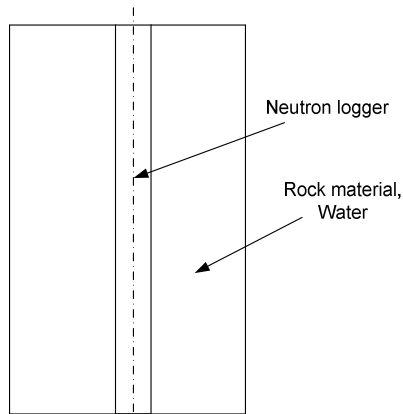


Figure 37: Neutron experiment setup giving the results in Figure 36.



**Figure 38: Sketch of proposed neutron logger experiment.**

Figure 38.

After these neutron logger experiments it was discussed how the experiment setup could be done differently and it was thought that emphasising on having the neutron logger in the centre would be the main parameter. The setup would be two pipes one just big enough for the neutron logger and a bigger pipe, concentric to the other pipe, for the rock material and water. The inner pipe could be made out of material that would not hinder the neutron from travelling into the rock material. A sketch of this setup can be seen in

## 5 Discussions

Using X-rays to detect and quantify water in steel pipes has not been performed before in the way it is done in this project. Lund & Þráinsson did measurements (Á. E. Lund & Þráinsson, 2003) in the field where one of the gathering pipes at the geothermal power plant in Svartsengi was studied using the same equipment as was done here. In Lund and Þráinsson (2003) experiment the X-ray equipment was setup to get an image from the side of the pipe and therefore the flow in the pipe could be seen rising on the video screen indicating slug flow of the two phases. The diameter of the gathering pipe was much larger than the X-ray equipment could cover so the experiment had to be done in three sections to cover the entire diameter. Nothing could be seen while the lower part of the pipe was the subject which was probably because the image was captured below the water level in the two phase flow inside the pipe. When the image was captured at the middle of the pipe, the surface of the water flow became visible (Á. E. Lund & Þráinsson, 2003).

Most of previous experiments, discussed in Introduction, that have used X-rays have either been, for example, for medical purposes, non destructive research of metal objects or used low attenuating plastic material. At least one used thin aluminium casing while using CT scan to measure water saturation in porous material (Dastan, 2006).

The X-ray equipment used in this project was manufactured for medical applications and not at all for industrial purposes. Although it is not designed for making X-ray images using steel pipes it worked quite well for pipe nr. 4 as described in Section 4.4. The main tasks of this project as stated in the Section 1 have all been covered in this project. It has been shown that the X-ray equipment available at the Biomedical engineering lab of Reykjavík University can

be used to detect and quantify water in steel pipes up to a certain limit, mostly determined by the wall thickness of the pipes. Even though it would have been preferred that the equipment available would have been more powerful than it was and more manual adjustment of the machine wanted, still it managed to penetrate pipe nr. 4 quite well. Pipe nr. 4 had wall thickness of 4,5 mm and from experiments with that pipe it was shown that 1 mm of steel is equivalent to 24 mm of water.

This project has shown that X-rays can be used to detect and quantify water saturation in steel pipes and it is also clear that the wall thickness of the pipe is a limiting factor in the experiments. If there is no rock material inside the pipe the diameter of the pipe becomes irrelevant because the attenuation of air and water inside the pipe is insignificant or very small, compared to the attenuation of the steel. If there is rock material inside the pipe the diameter becomes a parameter that needs to be taken into consideration when selecting size of the pipe because the X-ray equipment has to have enough power to penetrate the pipe and the rock material inside the pipe.

If pipe nr. 4 that fitted best to the X-ray equipment had been equipped for having two-phase flow of water and steam going through it, the maximum available pressure of the flow was calculated. To find out how much pressure pipe nr. 4 can withstand if two phase flow of water and steam was run through it, the following parameters were used: temperature at 150°C, the pipe having steel grade 235GH, wall thickness 4,5 mm and outer diameter of 76,2 mm. Using equation from EN 13480 standard and rearranging it so it gives the pressure:

$$p_c \leq \frac{2ef_c}{D_o - e} \quad (10)$$

Where  $p_c$  is pressure in MPa,  $f_c$  is design stress,  $e$  is wall thickness and  $D_o$  is outer diameter. To find the design stress  $f_c$  the minimum proof strength  $R_{p0,2t}$  for selected temperature is divided with 1,5 so the design stress is  $187 \text{ MPa} / 1,5 = 125 \text{ MPa}$ . Putting all the variables into eq. 11 gives 15,6 MPa which is then the maximum pressure it can safely withstand at 150°C. This shows that using steel pipes instead of plastic pipes allows experimenting at much higher pressure than plastic pipes can withstand.

- Measuring water saturation of two-phase flow in steel pipes using X-rays and the equipment available at the Biomedical engineering lab at Reykjavík University is possible.
- Limiting factors are the wall thickness of the pipe, in this project it was 4,5 mm and the power output of the X-ray equipment which was 6,4 mAs and 106 kVp in this project.

- X-rays have previously been used to measure water saturation using pipes made of plastic materials but it has been shown here that it can be measured at higher pressure in pipes made of steel, which is much more realistic when mimicking conditions in geothermal reservoirs.



## 6 References

- Ambusso, W. J. (1996). *Experimental determination of steam water relative permeability relations* (M.Sc. Thesis No. SGP-TR-154) (p. 80). Stanford, California: Stanford University.
- Corey, A. T. (1954). The interrelation between gas and oil relative permeabilities. *Producers Monthly*, 19(1), 38-41.
- CT physics: The Physics of computed tomorrow*. (2006). Retrieved from <http://www.lbl.gov/images/MicroWorlds/EMSpec.gif>
- Dastan, A. (2006). *Direct measurement of In-Situ Water Saturation in Geothermal Rocks* (Technical report No. SGP-TR-180). Stanford Geothermal Program.
- DiPippo, R. (2008). *Geothermal power plants: principles, applications, case studies and environmental impact*. Butterworth-Heinemann.
- Ellis, D. V. (1990). Some insight on neutron measurements. *IEEE*, IEEE Transactions on nuclear science, 37(no. 2), 959 - 965.
- Ellis, D. V., & Singer, J. M. (2008). *Well Logging for Earth Scientists* (2nd ed.). Springer.
- Fridleifsson, I. B., & Freeston, D. H. (1994). Geothermal energy research and development. *Geothermics*, 23(2), 175-214. doi:10.1016/0375-6505(94)90037-X
- Gudjonsdottir, M. S., Harvey, W., Palsson, H., & Saevarsdottir, G. (2010). Assessing relative permeabilities of two phase flows of water and steam in geothermal reservoirs: state of the art relations. *GRC Transaction* (Vol. 34, p. 4). Presented at the Celebrating 50 years of clean, renewable power, San Diego: GRC.
- Hessenbruch, A. (2002). A brief history of x-rays. *Endeavour*, 26(4), 137-141. doi:10.1016/S0160-9327(02)01465-5
- Horne, R. N., Satik, C., Mahiya, G., Li, K., Ambusso, W., Tovar, R. A., & Nassori, H. (2000). Steam-Water Relative Permeability, *I*(4), 597-604.

- Hurlock, G. S., Higashino, H., & Mochizuki, T. (2009). History of cardiac computed tomography: single to 320-detector row multislice computed tomography. *The International Journal of Cardiovascular Imaging*, 25(15695794), 31-42.  
doi:10.1007/s10554-008-9408-z
- Lawrence Berkeley National laboratory. (n.d.). Retrieved from  
<http://www.lbl.gov/images/MicroWorlds/EMSpec.gif>
- Lund, Á. E., & Þráinsson, S. (2003, December). *Tvífasa safnæðar - Two phase gathering pipes*. Reykjavík.
- Lund, J. W. (2004). 100 Years of geothermal power production. *Geo-Heat Center quarterly bulletin*, 25(3), 11-19.
- Mahiya, G. F. (1999). *Experimental Measurement of Steam-Water Relative Permeability*. STANFORD UNIVERSITY.
- Multimedia | USB Audio/Video Grabber. (n.d.). *Encore Electronics*. Homepage of a company, . Retrieved December 9, 2011, from <http://www.encore-usa.com/us/product/ENMVG>
- Murray, S. H. (1990). Computed tomography used in weld inspections at NASA. *NDT & E International*, Welding journal, 69(2), 129. doi:10.1016/0963-8695(96)84079-5
- Röntgen, W. C. (1896). On a new kind of rays. *Nature*, 53(1369), 274-276.  
doi:10.1038/053274b0
- Sanders, R. (2003, December 10). Radioactive potassium may be major heat source in Earth's core. Press release, . Retrieved December 30, 2011, from  
[http://www.berkeley.edu/news/media/releases/2003/12/10\\_heat.shtml](http://www.berkeley.edu/news/media/releases/2003/12/10_heat.shtml)
- Satik, C. (1998). A measurement of steam and water relative permeability (pp. 120-126). Presented at the Stanford Geothermal Workshop, Stanford, California: Stanford University.

- Schembre, J. M., & Kavscek, A. R. (2003). A technique for measuring two-phase relative permeability in porous media via X-ray CT measurements. *Journal of Petroleum Science and Engineering*, 39(1-2), 159-174. doi:10.1016/S0920-4105(03)00046-9
- Siegbahn, K. (1955). *Beta- and gamma-ray spectroscopy*. Interscience Publishers.
- Simmons, A. (n.d.). *x-ray\_tube*. Retrieved from [http://www.genesis.net.au/~ajs/projects/medical\\_physics/graphics/x-ray\\_tube.jpg](http://www.genesis.net.au/~ajs/projects/medical_physics/graphics/x-ray_tube.jpg)
- Sternheim, M. M., & Kane, J. W. (1991). *General Physics* (2nd ed.). New York: Wiley & sons.
- Suetens, P. (2009). *Fundamentals of Medical Imaging* (2nd ed.). Cambridge University Press.
- Wang, G., & Liao, T. W. (2002). Automatic identification of different types of welding defects in radiographic images. *NDT & E International*, 35(8), 519-528. doi:10.1016/S0963-8695(02)00025-7
- Wolbarst, A. B. (2005). *Physics of radiology* (second.). Madison WI: Medical Physics Publishing.